3-2005

Analysis of Computational Methods for the Treatment of Material Interfaces

Minh C. Nguyen

ANALYSIS OF COMPUTATIONAL METHODS FOR THE TREATMENT OF MATERIAL INTERFACES

THESIS

Minh C. Nguyen, Captain, USAF

AFIT/GAE/ENY/05-M15

DEPARTMENT OF THE AIR FORCE
AIR UNIVERSITY

AIR FORCE INSTITUTE OF TECHNOLOGY

Wright-Patterson Air Force Base, Ohio

The views expressed in this thesis are those of the author and do not reflect the official policy or position of the United States Air Force, Department of Defense, or the United States Government.

AFIT/GAE/ENY/05-M15

ANALYSIS OF COMPUTATIONAL METHODS FOR THE TREATMENT OF MATERIAL INTERFACES

THESIS

Presented to the Faculty

Department of Aeronautics and Astronautics

Graduate School of Engineering and Management

Air Force Institute of Technology

Air University

Air Education and Training Command

In Partial Fulfillment of the Requirements for the

Degree of Master of Science in Aeronautical Engineering

Minh C. Nguyen, BS

Captain, USAF

March 2005

AFIT/GAE/ENY/05-M15

ANALYSIS OF COMPUTATIONAL METHODS FOR THE TREATMENT OF MATERIAL INTERFACES

Minh C. Nguyen, BS

Captain, USAF

Approved:

//*signed*//	20050311
Dr Anthony N. Palazotto (Chairman)	Date
//*signed*//	20050311
Dr William P. Baker (Member)	Date
//*signed*//	20050311
Dr Theodore Nicholas (Member)	Date

Abstract

The issue of high speed impact and hypervelocity gouging in particular is of great interest to the Air Force Office of Scientific Research and the Air Force Research Laboratory's Holloman High Speed Test Track. Rocket sled tests at the facility frequently approach velocities where concern for gouging development becomes the limiting factor to achieving higher operating velocities. Direct observation of the gouging process is not possible so computational modeling is necessary to study the phenomenon. Since gouging development is dependent on the impact surface conditions, the method used to model material interfaces directly affects the accuracy of the solution.

This research is primarily interested in the methods for modeling material interfaces available in CTH, a hydrocode developed by Sandia National Laboratories. Three methods are available in CTH to handle material interfaces: 1) materials are joined at the interface, 2) a frictionless slide line is inserted, and 3) a boundary layer interface is established. An axisymmetric impact scenario is used to explore these methods and their influence on high energy impact solutions. The three methods are also compared in an axisymmetric sliding scenario.

The method of joining materials at the contact surface appears well suited to the simulation of high energy impact events and hypervelocity gouging. In general, the frictionless slide line method introduces numerical instability. Finally, the boundary layer interface method is too limited for two dimensional applications.

Acknowledgments

I would like to express my sincere appreciation to my faculty advisor, Anthony N. Palazotto, for his guidance and support throughout the course of this thesis effort. The insight and experience was certainly appreciated. I would also like to thank the members of my thesis committee, Dr William P. Baker and Dr Theodore Nicholas, for their time and patience. This research has been sponsored by the Air Force Office of Scientific Research with Dr. Neal D. Glassman as program manager.

Minh C Nguyen

Table of Contents

Page

Page

List of Figures

Page

Page

Page

List of Tables

Page

ANALYSIS OF COMPUTATIONAL METHODS FOR THE TREATMENT OF MATERIAL INTERFACES

I. Introduction

Background

The Holloman High Speed Test Track (HHSTT) is a ground-based test facility operated by the US Air Force for the testing of various hardware systems in simulated free flight conditions. The facility conducts tests using rocket propelled sleds that ride along continuous steel rails which span a distance of 50,988 feet. The rocket sleds are guided along the rail by steel slippers which maintain a small gap with the rail to allow for limited free flight. Upgrades to the facility have allowed tests to be conducted at extremely high velocities approaching 1-2 km/s with plans presently developed that would allow for a velocity of 3km/s. At these velocities, the free flight conditions allow for the possibility that the slippers will impact the rail due to roll, pitch, or yaw motions experienced by the test sled. The severity of the impact varies but in certain cases can result in the loss of the test sled. Inspections of the rails after test events have revealed damage in the form of gouges. Gouges associated with high energy impacts are characterized by a teardrop shaped shallow depression in the material along with a raised hump at the blunt end of the gouge. Figure 1 shows a diagram of a typical gouge.

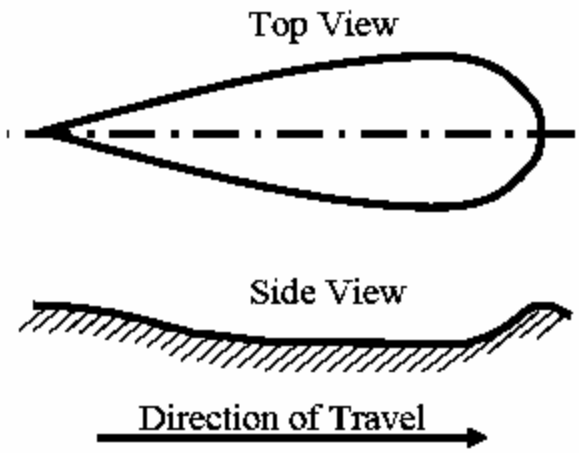

Figure 1.1 Illustration of a Gouge

A hypothesis for the hypervelocity gouging process was offered by Barber and Bauer [2] which attributed gouge formation to microscopic surface asperity impact between a moving slider and a stationary rail. The impact is characterized as a discrete, localized, and violent event. The energy released in such an impact would resemble a microscopic explosion and produce a small crater at the surfaces of the contacting solids. The relative motion of the slider imparts a velocity to the center of mass of the explosion of approximately one-half of the slider velocity. The motion of the center of mass of the explosion as it expands results in the characteristic teardrop shaped gouge which is formed in both the slider and the rail.

Computational Hypervelocity Gouging Research

The hypervelocity gouging process, as it pertains to the HHSTT, was successfully simulated by Laird and Palazotto [10] using the hydrocode CTH. They were able to observe the development of a gouge and identify the mechanisms that lead to gouge

formation. Two conditions were reported as necessary for gouge initiation. First, the slipper must penetrate into the rail, through a vertical impact or a horizontal impact with an asperity. Secondly, the slipper must maintain sufficient horizontal velocity after penetration to produce stresses exceeding the flow stress of both the slipper and rail materials. The resulting plastic flow takes the form of material jets which continually grow and penetrate further into the two surfaces, initiating a gouge. The gouge grows in the direction of the slipper velocity but at one half of the magnitude of the slipper velocity. The length and depth of the resulting gouge are proportional to the length of the slipper and the amount of time required for the slipper to move past the gouge. A typical gouge being developed is shown in Figure 1.2.

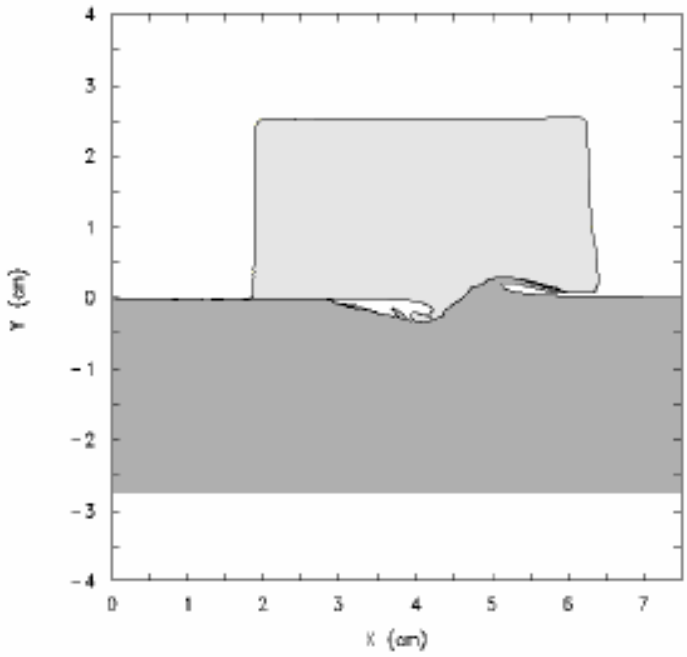

Figure 1.2 Gouge Simulation by Laird [9]

Similar research was also conducted by Szmerekovsky [14] in which the capabilities of three computational tools to simulate hypervelocity gouging were

evaluated. The hydrocode CTH was the only software package which employed an Eulerian Finite Volume solution method. ABAQUS and LS-DYNA3D were the other two software packages and both employed a Lagrangian Finite Element solution method. The following 11 criteria were used by Szmerekovsky to evaluate the three computational tools and determine which was most suitable for numerical simulation of the hypervelocity gouging phenomenon [14].

1. Mesh capabilities and their ability to capture the large deformations and high strain rates of the gouging phenomenon without excessive distortion.
2. Availability of equation of state and constitutive model capabilities.
3. Representation of failure and availability of failure models.
4. Ability of the solution methods and material models to accurately model high energy impact phenomena such as normal shock waves.
5. Availability of models for heat flux and heat flow due to deformation.
6. Availability of contact and material mixing algorithms.
7. Capability to model conditions (e.g., plastic zone, shear bands, and high pressure core) that lead to gouging.
8. Capability to model interacting material “jets” and ejecta associated with gouging.
9. Availability of the code on readily accessible high performance computational platforms.
10. Availability of technical support.
11. Previous work done on similar problems.

This study revealed that both ABAQUS and LS-DYNA3D had difficulties in modeling the large deformations involved in the gouging process. This was attributed to an inherent limitation of the Lagrangian mesh used by these software packages. CTH was determined to be the best tool available for the numerical investigation of hypervelocity gouging.

The gouging model developed by Laird was further refined by Szmerekovsky [14] to relate numerical results directly back to experimental test conditions at the

HHSTT. A dimensional analysis and similitude study was conducted to facilitate the creation of CTH models based on actual test sled configurations. In addition to establishing which physical dimensions and characteristic parameters influence the initiation of gouging, Szmerekovsky also considered factors for the mitigation of gouging, specifically the use of coatings. His results reflect the successful use of coatings at the HHSTT where an epoxy coating is applied to the rail in the region where the test sled is expected to reach its highest velocities as a gouging mitigation measure.

Problem Statement and Objectives

At the HHSTT, a significant portion of the rail is not coated and observations of rocket sled tests suggest that friction may have a significant role in the development of conditions conducive to gouging formation. Whether frictional effects can be accounted for with a CTH model is the concern. This issue is tied to the method used to define material interfaces, and this research effort explores the methods available in CTH.

II. Theory and Literature Review

Chapter Overview

This chapter provides background theory concerning friction and hydrocodes, with a focus on CTH and its boundary layer algorithm. Also presented in this chapter are previous research efforts in the fields of friction and high energy impact.

Friction

Friction is a force between two surfaces, parallel to the interface, and opposing relative motion. Four general mechanisms are presented by Bayer [3] as the basis for friction between two solids: adhesion, abrasion, hysteresis, and viscous losses. Adhesive friction arises from the force required to shear bonded junctions that form between two surfaces. Similarly, abrasive friction is associated with the force required to deform the surfaces or to cut a groove or chip. Hysteresis is a product of repeated-cycle deformations and takes into account that real materials are not perfectly elastic. Energy is dissipated in each stress cycle, with the effect of either asperity deformation on a micro scale or deformation of the overall geometry of the solids. Friction due to viscous losses occurs when a fluid or lubricant is placed between the two surfaces. The magnitude of the friction force F can be expressed as a sum of these 4 components and a corresponding expression for the coefficient of friction, μ, can be obtained by dividing through by the normal force, N:

$$F = F_{ad} + F_{ab} + F_{hys} + F_{vis} \tag{2.1}$$

$$\mu = \frac{F}{N} = \mu_{ad} + \mu_{ab} + \mu_{hys} + \mu_{vis} \tag{2.2}$$

where subscripts ad, ab, hys, and vis are the components of friction relating to adhesion, abrasion, hysteresis, and viscous losses respectively.

Each component of friction contributes in varying quantities that are dependent on the physical scenario, but they result in the same overall effect. This effect is the dissipation of energy, a most significant aspect of friction. The energy dissipating effect of friction occurs through the generation of heat and material deformation. Bayer asserts that the dominant process is the generation of heat, which accounts for over 90% of the energy dissipated. While the 4 components of friction are conceptually unique, the process of identifying the specific contribution of each component in a physical scenario is often difficult. In a hypervelocity gouging scenario, it would be reasonable to expect that only the mechanisms of adhesion, abrasion, and viscosity contribute to the friction force.

Experimental work was conducted by Bowden and Freitag [6] in 1958 to characterize friction between metal surfaces at velocities up to 800 m/s. In these experiments, coefficients of friction were established for steel on copper, aluminum, duralumin, bismuth, antimony, and molybdenum. The experiment made use of a steel sphere suspended in a magnetic field and accelerated by a rotating magnetic field. The freely spinning sphere was then decelerated through contact with three symmetrically arranged flat plates of the dissimilar material of interest. The friction force was calculated by measuring the deceleration of the sphere. The friction coefficient was then calculated by dividing the calculated friction force by the known normal force applied by

the three flat plates. While actual friction coefficients were highly dependent on the materials involved, the results showed a clear trend of decreasing coefficient with increasing velocity in all cases. The data fitted curves also suggested some minimum coefficient of friction greater than zero was reached asymptotically that varied from as high as .20 for steel on aluminum to as low as .05 for steel on bismuth.

Hydrocodes

The primary tool used in this research is CTH, a hydrocode produced by Sandia National Labs. A hydrocode is a software package developed to numerically simulate highly dynamic events involving shocks. Anderson [1] presents an informative overview of this class of computer programs which are capable of simulating the propagation of shockwaves and computing properties such as velocities, stresses, strains, and energy as functions of space and time. To accomplish this, hydrocodes solve a discretized set of the conservation equations of mass, momentum, and energy, an equation of state, a material constitutive model, and a material failure model. Two fundamental approaches to the solution of the conservation equations exist: the material based Lagrangian approach and the spatially based Eulerian approach. This historically resulted in two distinct subclasses of hydrocodes whereas modern hydrocodes such as CTH take a hybrid approach to realize the benefits of both the Lagrangian and the Eulerian methods.

Lagrangian hydrocodes employ a computational grid that is fixed to the material with initial connections between the grid points forming cells of constant mass. The computational grid need only be generated where material actually exists in the defined problem space. The grid points are constrained to move with the local material velocity

and values such as velocity, pressure, density, and temperature are calculated for each grid point at each time step throughout the solution process. The immediate advantage of this approach is the ability to clearly identify material boundaries and interfaces. This facilitates the process of defining boundary conditions at free surfaces as well as contact surfaces. The frictional effects at the contact surfaces can also be readily captured. Significant disadvantages of a material fixed grid reveal themselves in large deformation problems as time progresses. Issues of grid distortion and cell compression can produce computing difficulties as well as significant errors. The extreme case of grid distortion where negative area/volume cells result will halt the solution process. In a hypervelocity impact scenario this could manifest very early (first few microseconds) in the solution process due to large deformations at the contact surface. Extreme cell compression forces the hydrocode to reduce the time step resulting in an overall computational time that may not be acceptable or feasible. To proceed with the solution would require a new computational grid to be overlaid with properties calculated from the distorted grid, keeping in mind the need to conserve mass, momentum, and energy. Material mixing in the impact region would also not be captured by a Lagrangian hydrocode since mixed material cells are not possible.

Eulerian hydrocodes avoid the problems of grid distortion and cell compression through the use of a spatially fixed grid which results in fixed volume cells. However, the computational grid must be defined for the entire problem space, including originally empty regions to which material may propagate as the solution progresses. This approach computes the flow of mass, momentum, and energy across the cell boundaries.

Since mass flow through the cells is permitted, this approach accommodates problems involving material diffusion and mixing. The mixing of material at contact surfaces can be accurately modeled. However, this ability to handle mixed cells can result in ambiguous material boundaries and interfaces. No distinct material boundaries exist within a given cell, complicating the task of applying boundary conditions. To reduce the impact of this, smaller grid point spacing can be applied at the expense of increased computation time. With no distinct material interfaces, the study of friction on contact surfaces becomes more arduous and less accurate.

CTH

The hydrocode CTH was developed at Sandia National Laboratories to handle 3-D, multi-material, large deformation, strong shock problems [11]. CTH employs an Eulerian mesh where all quantities are cell centered except for the face centered velocities. The two-step Eulerian solution scheme used by CTH involves a Lagrangian step followed by a remap step and is second order accurate.

In the Lagrangian step, the mesh is allowed to distort with the material. During this step, conservation of volume, mass, momentum, and energy are conserved. Since the mesh is fixed to the material in this step, mass is conserved automatically. The governing equations are replaced with explicit finite volume approximations. However, solution of these equations requires a timestep small enough to limit the volume change in individual cells and to limit the distance a wave can travel to less than one cell width.

The second step remaps the distorted cells back to the original Eulerian mesh. The volume flux between cells is calculated first based on the cell face velocities. A

high-resolution interface tracker algorithm is then implemented to ensure the right materials are moved with the volume. Each material's corresponding mass, momentum, and energy are then moved.

CTH relies heavily on graphics to present results to the user but data from tracer points can also be obtained. These tracer points, which can be Eulerian or Lagrangian, need to be defined before the problem is submitted to CTH for solution. Some knowledge of the expected regions of interest/activity is necessary for the strategic placement of these points. Data for the rest of the defined mesh can be obtained through the use of contour and vector plots. The data range for such plots is defined by the user, so some knowledge of the expected results along with trial and error is necessary to generate meaningful results with the graphical post processing capability.

Boundary Layer Algorithm

CTH was originally developed to simulate problems involving strong shock waves where pressures are very large but shear stresses are relatively small. Under this premise, two simplified options were implemented for the treatment of effects at material interfaces. The default option is to assume materials are joined at their contact surface by requiring the velocity be constant across the interface. The second option is the slide line approach. Before further discussion regarding this approach, it should be noted that the state of stress at a point can be represented by the Cauchy stress tensor which can be expressed in terms of a spherical component and a deviatoric component as follows [12]:

$$\begin{bmatrix} \sigma_{11} & \sigma_{12} & \sigma_{13} \\ \sigma_{12} & \sigma_{22} & \sigma_{23} \\ \sigma_{13} & \sigma_{23} & \sigma_{33} \end{bmatrix} = \begin{bmatrix} \sigma_m & 0 & 0 \\ 0 & \sigma_m & 0 \\ 0 & 0 & \sigma_m \end{bmatrix} + \begin{bmatrix} \sigma'_{11} & \sigma_{12} & \sigma_{13} \\ \sigma_{12} & \sigma'_{22} & \sigma_{23} \\ \sigma_{13} & \sigma_{23} & \sigma'_{33} \end{bmatrix} \qquad (2.3)$$

where σ_m is the mean stress or pressure and is define as:

$$\sigma_m = \frac{\sigma_{11} + \sigma_{22} + \sigma_{33}}{3} \tag{2.4}$$

Continuing on, the alternate slide line approach designates the contact surface as a frictionless sliding interface by setting the material strengths, and hence the deviatoric stress, of mixed material cells to zero. Only pressure is supported by these mixed cells. Even with a model that initially aligns the material surfaces with the grid lines, as the materials make contact and deform, the material interfaces will shift into the cell interiors and result in mixed material cells as shown in Figure 2.1. The slide line approach can have the effect of reducing the strength of a projectile surface since that surface is treated as a fluid. This fluid layer can be swept away as the projectile penetrates a target resulting in a distorted projectile shape. This was an acceptable result for the impact studies of interest when CTH was originally developed, since erosion of the projectile surface and deformation of the projectile in general as it penetrated the target was experimentally observed. However, interest in lower velocity penetration and perforation problems, below 1.5 km/s, have become a subject of interest and in these scenarios, significant deformation of the projectile is not physically observed. CTH simulations of these low velocity penetration events using the slide line approach can produce erroneous results by showing projectile deformation which may not reflect physical phenomena.

In an attempt to more accurately simulate low speed penetration and perforation problems, a boundary layer algorithm was developed to improve the way CTH handles sliding interfaces [13]. Since this algorithm was developed for these particular problems, its implementation in CTH is limited in 2D to axisymmetric problems. The basic

approach of the boundary layer algorithm is to move the sliding interface into the target material. This eliminates the purely numerical effect of erosion of the penetrator surface.

The first phase of the boundary layer algorithm identifies cells in two distinct layers, a hard boundary layer and a soft boundary layer. Within these boundary layers lies the interface layer which contains the actual contact surface. Within the soft boundary layer lies the slip layer which is the artificial sliding surface.

The interface layer is defined first. CTH calculates the material volume fractions, ϕ_h and ϕ_s, corresponding to the hard and soft materials respectively, for each mesh cell. To locate the material interface, the components of the vector gradients $\nabla\phi_h$ and $\nabla\phi_s$ are then calculated using central difference formulas:

$$(\nabla\phi_{hx})_{i,j} = \frac{(\phi_h)_{i+1,j} - (\phi_h)_{i-1,j}}{2\Delta x}\ ,\ (\nabla\phi_{hy})_{i,j} = \frac{(\phi_h)_{i+1,j} - (\phi_h)_{i-1,j}}{2\Delta y} \tag{2.5}$$

$$(\nabla\phi_{sx})_{i,j} = \frac{(\phi_s)_{i+1,j} - (\phi_s)_{i-1,j}}{2\Delta x}\ ,\ (\nabla\phi_{sy})_{i,j} = \frac{(\phi_s)_{i+1,j} - (\phi_s)_{i-1,j}}{2\Delta y} \tag{2.6}$$

in which Δx and Δy are the cell widths and the subscripts i,j indicate the cell coordinates. Figure 2.1 illustrates a typical mesh with cell coordinates for a representative mesh region indicated. Cells in which both the $\left|(\nabla\phi_h)_{i,j}\right| \geq 0.1$ and $\left|(\nabla\phi_s)_{i,j}\right| \geq 0.1$ define the interface layer. This normally results in a layer that is two to three cells thick depending where the physical material interface is in relation to the cell edges. Figures 2.2 and 2.3 illustrate the cases where the physical material interface does or does not line up with cell edges. The latter case establishes mixed material cells from the start. An effective unit normal

vector $\mathbf{n}_{i,j}$, which is perpendicular to the material interface and points into the hard material, is also calculated for each cell in the interface layer as shown in Figures 2.2 and 2.3:

$$\mathbf{n}_{i,j} = \frac{(\nabla\phi_h)_{i,j} - (\nabla\phi_s)_{i,j}}{\left|(\nabla\phi_h)_{i,j} - (\nabla\phi_s)_{i,j}\right|} \tag{2.7}$$

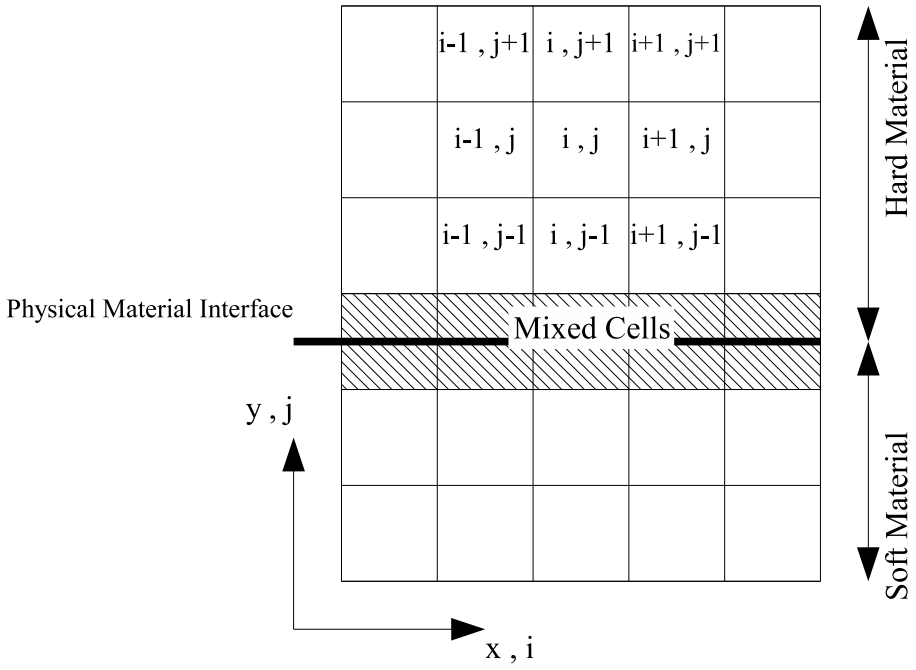

Figure 2.1 Typical Mesh Showing Sample Cell Coordinates

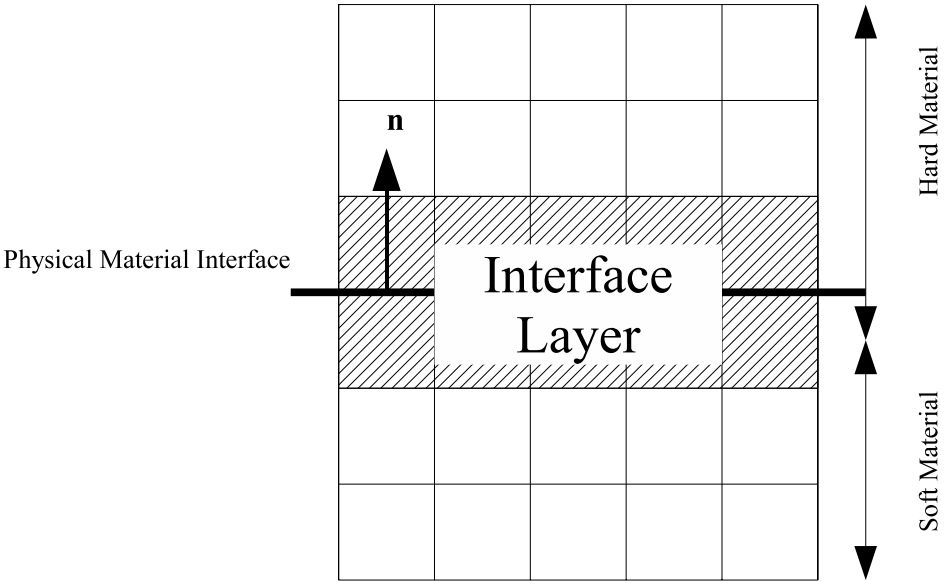

Figure 2.2 Interface Layer, Material Interface Aligned With Cell Edge

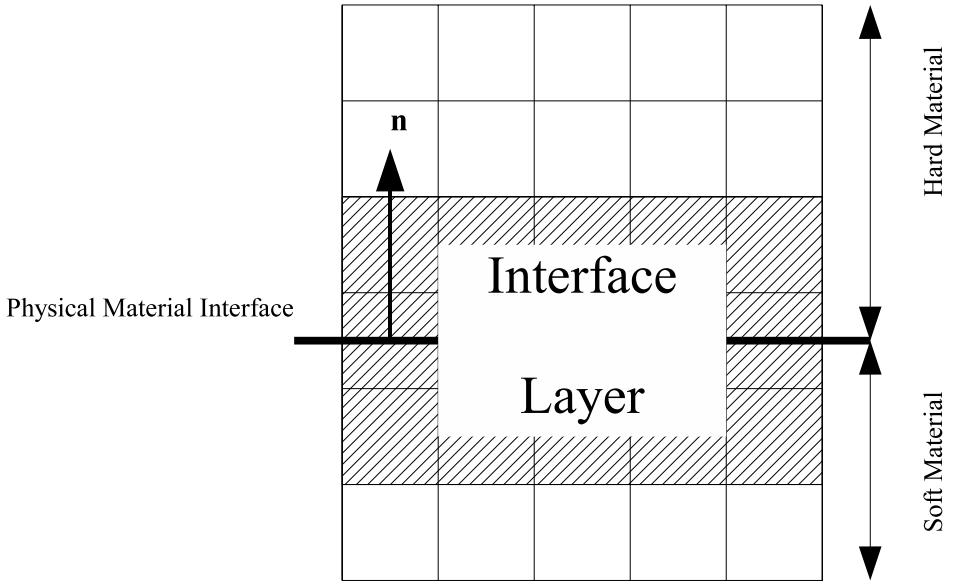

Figure 2.3 Interface Layer, Material Interface Inside Cells

The two boundary layers are defined next. A cell is in one of the boundary layers if its cell center is within some user defined distance, w_{bl}, of an interface layer cell. If the

cell also has a soft material volume fraction, ϕ_s, of at least .99, than it is in the soft boundary layer. Otherwise, it is in the hard boundary layer. This effectively designates almost all mixed material cells as hard boundary layer cells.

Finally, the slip layer is defined as those cells in the soft boundary layer that are also within some user defined distance, w_{sl}, of an interface layer cell. The slip layer models a frictionless sliding interface by setting the deviatoric stress to zero.

Shown in figures 2.4 and 2.5 are the boundary layer configurations for the cases where the physical material interface does or does not align with the cell edges. In the latter case, the hard boundary layer actually contains the mixed material cells, effectively increasing the size of the penetrator. These mixed cells also have their yield stress set to the hard material yield stress to prevent nonphysical erosion of the hard material as happens with the slide line method.

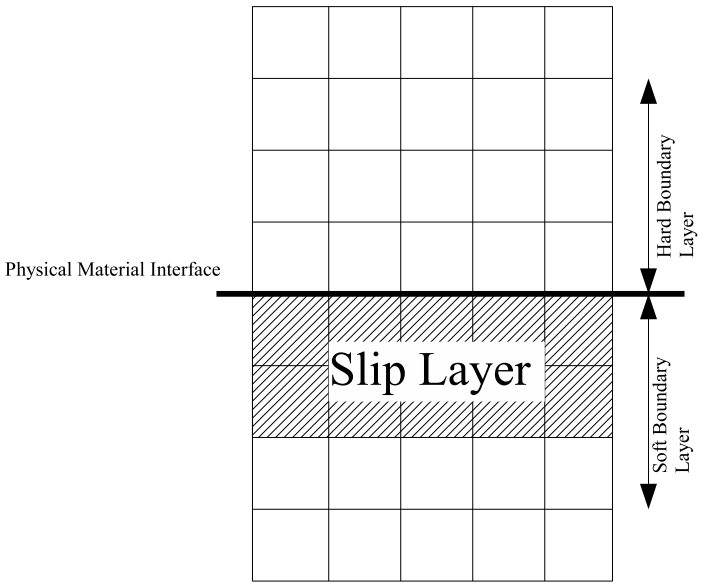

Figure 2.4 Boundary Layers, Material Interface Aligned With Cell Edge

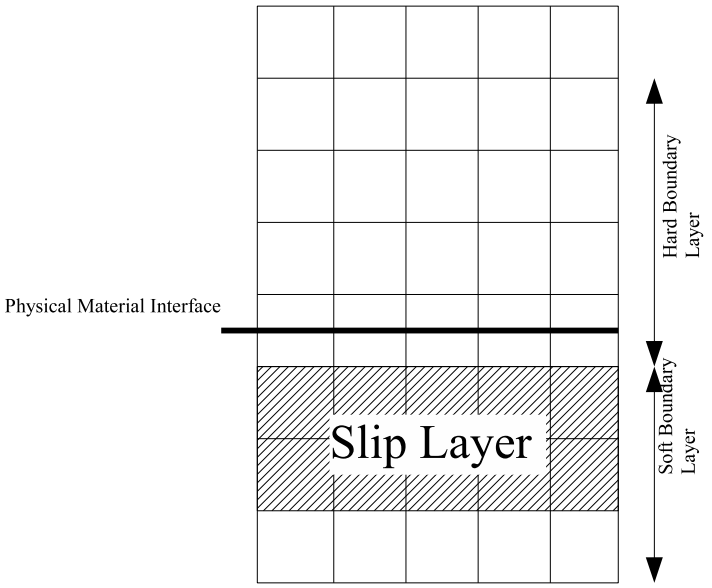

Figure 2.5 Boundary Layers, Material Interface Inside Cells

The second phase of the Boundary Layer Algorithm calculates friction forces for cells that exist in either Boundary Layer but not the Interface Layer, which, in general, contain mixed material cells. Friction forces are not applied to Interface Layer cells due to limitations in CTH's ability to handle mixed material cells. Friction is not applied as a direct force which would contribute to the deviatoric stress but rather as a body force that contributes to the momentum balance. This friction body force is computed as follows.

For each cell in one of the boundary layers, an average velocity of the hard material, $\mathbf{V}_h$, and an average velocity of the soft material, $\mathbf{V}_s$, is calculated. Contributing values are typically taken from cells within an approximate 5 cell radius, disregarding slip layer cells which may not accurately reflect the bulk motion of the soft material. The relative velocity vector of hard and soft material for each cell is then evaluated from:

$$\overline{V} = V_h - V_s \tag{2.8}$$

Similarly the average unit normal vector, $\bar{n}$, and the average Cauchy stress tensor, $\bar{T}$, for each cell are calculated from the same contributing cells. Since $\bar{V}$ may not necessarily be tangential to the contact surface, a unit vector, **u**, which is tangential to the contact surface and points in the direction of the friction force acting on the soft material, as shown in Figure 2.6, is calculated:

$$\mathbf{u} = \frac{(\bar{n} \times \bar{V}) \times \bar{n}}{\left|(\bar{n} \times \bar{V}) \times \bar{n}\right|} \tag{2.9}$$

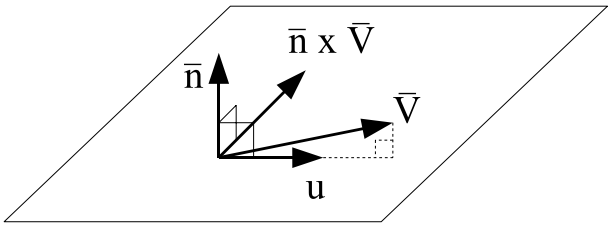

Figure 2.6 Diagram of Unit Vector **u**

The shear traction vector $\mathbf{t}_f$ is then calculated from

$$\mathbf{t}_f = \pm f \min\{0\ ,\ \bar{n} \cdot (\bar{T}\bar{n})\}\mathbf{u} \tag{2.10}$$

where f is the user defined coefficient of friction and the scalar quantity $\bar{n} \cdot (\bar{T}\bar{n})$ is the component of stress in the direction of $\bar{n}$, also referred to as the normal traction, and can also be expressed in matrix notation as:

$$\bar{n} \cdot (\bar{T}\bar{n}) = \begin{bmatrix} \bar{l}_1 & \bar{l}_2 & \bar{l}_3 \end{bmatrix} \cdot \begin{bmatrix} \bar{\sigma}_{11} & \bar{\sigma}_{12} & \bar{\sigma}_{13} \\ \bar{\sigma}_{12} & \bar{\sigma}_{22} & \bar{\sigma}_{23} \\ \bar{\sigma}_{13} & \bar{\sigma}_{23} & \bar{\sigma}_{33} \end{bmatrix} \begin{bmatrix} \bar{l}_1 \\ \bar{l}_2 \\ \bar{l}_3 \end{bmatrix} \tag{2.11}$$

For the shear traction to be nonzero, the normal traction must be compressive (negative value). The sign is negative if the cell is in the soft layer to produce a positive shear

traction acting on the soft material in the direction of **u**. The sign is positive if the cell is in the hard layer to produce a negative shear traction acting on the hard material opposition the direction of **u**. The shear traction is then converted to a body force density:

$$\mathbf{b}_f = \mathbf{t}_f / w_{bl} \tag{2.12}$$

which appears in the momentum balance equation:

$$\rho \mathbf{a} = \nabla \cdot \mathbf{T} + \mathbf{b}_f \tag{2.13}$$

in which ρ is the density, **a** is the acceleration, and **T** is the Cauchy stress tensor.

Due to issues of mesh coarseness and uncertainty in the contact surface shape which can affect the number of cells included in the interface layer, the amount of friction calculated at any given will fluctuate. Over time however, this fluctuation is averaged out and the net friction force applied to the solution approaches the correct amount.

To apply the boundary layer algorithm, the user must designate a hard material and a soft material for each pairing of materials that may come into contact and require a boundary layer interface to be defined. The width of the boundary layers can be defined by the user but is not necessary. Also, to explicitly add friction to a scenario, a coefficient of friction must be defined by the user.

An option also is available to artificially increase the yield stress of the hard material to prevent non physical plastic deformation of a projectile. This can occur if the applied shear stress is close enough to the material yield stress for numerical noise to be a concern.

The boundary layer algorithm also restricts material in the slip layer from flowing counter to the direction of the projectile which the user can override. The velocity component of material in the Slip Layer parallel to the projectile velocity vector is not permitted to be less than the projectile velocity. If counterflow is permitted in the slip layer, the algorithm can fail to compute that the projectile ever comes to rest since target material would continually be ejected from the slip layer.

To validate the improvements made to CTH with the implementation of the boundary layer algorithm, Silling [13] developed several test cases to compare CTH solutions to available experimental data. One case of interest simulates the deep penetration of an aluminum target by a hemispherical-nosed maraging steel rod. This case was experimentally investigated by Forrestal, Brar, and Luk [7]. The projectile was a T200 maraging steel rod of length 71.12mm and diameter 7.11mm. The target was a 6061-T651 aluminum cylinder of length 198mm and diameter 152mm. Material properties are presented in Table 2.1, where Y is the tensile yield stress, E is the modulus of elasticity, and ν is Poisson's ratio. The impact velocity was measured at 959m/s. For the CTH simulations, Silling employed a 2D axisymmetric model that contained the entire target and projectile. The projectile was modeled as an elastic perfectly plastic material but the target was modeled with the Johnson-Cook viscoplastic model. Both materials were modeled using a Mie-Gruneisen equation of state.

Table 2.1 Material Properties, Forrestal, Brar, and Luk Experiment

	T200 Maraging Steel	6061-T651 Aluminum
Y	1400 MPa	240 MPa
E	200 Gpa	68 GPa
ν	.31	.33

Experimental results indicated a penetration depth of 109mm. Inspection of the target material also revealed a thin layer along the inside of the resulting cavity that suggested the material had melted. The formation of the melted layer was assumed to be a frictional effect resulting from the contact between the target and the nose of the projectile. Silling obtained solutions using mesh cell sizes of .08cm and .04cm and a friction coefficient of .06. The .08cm mesh under predicted the depth at 102mm while the .04cm mesh over predicted the depth at 115mm.

III. Methodology

Chapter Overview

Presented in this chapter are the methods used to investigate the three methods employed by CTH to model material interfaces. The three methods will be referred to as 1) No Slide Line, 2) Slide Line, and 3) Boundary Layer. The first method is the default and assumes materials are joined at their contact surfaces. The Slide Line method establishes a frictionless sliding interface at the contact surfaces. The Boundary Layer method implements the boundary layer algorithm where the sliding interface is established in the target material. These three methods are compared in a normal impact scenario and a tangential sliding scenario.

Normal Impact, Part 1

The deep penetration model developed by Silling [13] to validate the boundary layer algorithm is used for the initial phase of this research and is illustrated in Figure 3.1. This axisymmetric model was defined in 2D cylindrical coordinates with a symmetry boundary condition at $x = 0$ and sound speed absorbing boundary conditions at the three remaining mesh boundaries. The sound speed absorbing boundary condition simulates a semi infinite boundary to prevent shock reflections back into the mesh [4]. This model was used to investigate four cases:

1. The model as provided, which employs the Boundary Layer method, to verify reproducibility of the reported results
2. The model employing the Slide Line method
3. The model employing the No Slide Line method

4. The Boundary Layer model with friction coefficient (μ) changed from 0.02 to 0.0

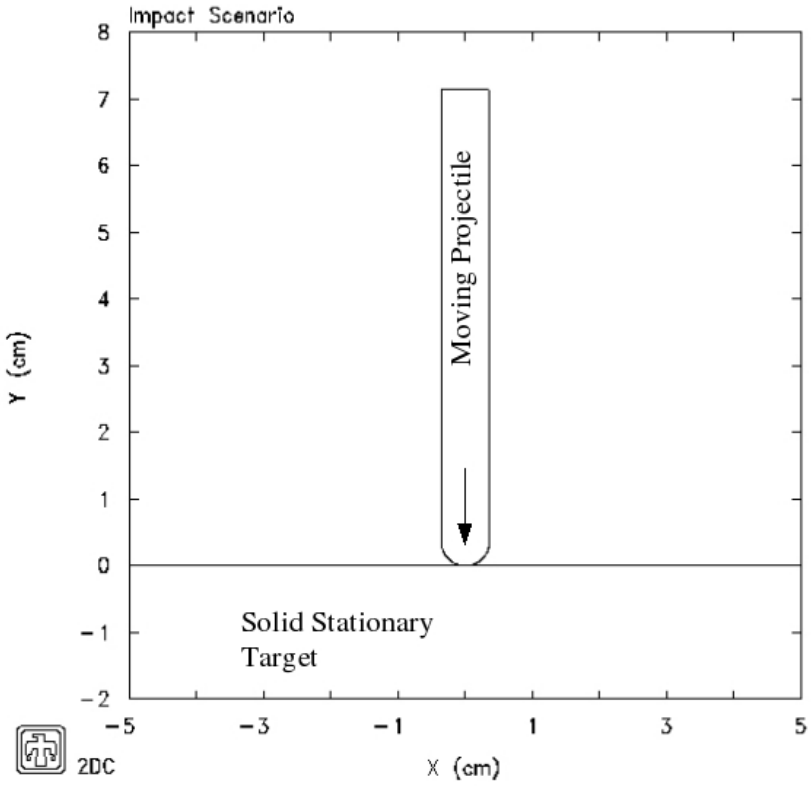

Figure 3.1 Graphic of Impact Scenario

These impact cases are studied to gain insight on how CTH handles material interfaces. The results are used to quantify the improvements that the boundary layer algorithm provides. The fourth case is expected to isolate the effect of shifting the sliding interface away from the actual material interface while still assuming frictionless sliding. These solutions were resolved out to 300 microseconds to ensure maximum penetration depths were achieved for comparison.

Lagrangian tracers are used to capture the conditions which develop at specific points along the contact surface between the projectile and target. The use of Lagrangian tracers is necessary since the contact surface moves with the projectile.

The original .04cm mesh was also further refined to a mesh cell size of .01cm. This was accomplished due to numerical artifacts observed at the original .04cm cell size. Solutions were obtained again using all three methods for defining material interfaces. The fourth case with coefficient of friction set to 0.0 was not solved with the refined mesh. The two Boundary Layer cases were sufficiently similar with the .04cm mesh that further investigation was not warranted. Also, since the boundary layer algorithm does not support data parallel computing, solutions were only resolved out to 50 microseconds since the finer meshes were significantly more computationally intensive and time consuming running on a single workstation. These solutions were also generating output data files approaching the 2GB size limitation imposed by CTH.

Normal Impact, Part 2

The deep penetration model was then modified to incorporate actual materials used at the HHSTT. The penetrator material was changed to a strain rate independent Steinberg-Guinan-Lund viscoplastic model of Vascomax 300. The target material was changed to a Johnson-Cook viscoplastic model of Iron, the most similar material model to 1080 steel available. Tabular equation of state data was also available for both materials. The material properties are presented in Table 3.1, where T_{melt} is the melting temperature. Solutions for all three material interface methods were obtained with a mesh size of .01cm. Since the penetration depths encountered with the change in

materials was significantly less, the overall mesh dimensions were reduced to allow solution times out to 100 microseconds.

Table 3.1 Material Properties, HHSTT

	Vascomax 300	1080 Steel	Iron
Y	2000 MPa	700 MPa	572 MPa
E	200 GPa	200 GPa	172 GPa
ν	.31	.25	.28
T_{melt}	1650 K	1835 K	1811 K

Pure Sliding

The final phase of this study attempts to isolate the frictional effects of a high energy impact by simulating a pure sliding scenario. The normal impact model used previously is modified by removing the material directly in the path of the projectile. This models a cylinder sliding inside a cylinder and is illustrated in Figure 3.2. The only contact surface in this scenario is parallel to the direction of motion however there is continuous contact along the length of the projectile. Shear forces on that surface should be purely a result of sliding friction. Solutions for a projectile velocity of 1km/s were resolved out to 50 microseconds.

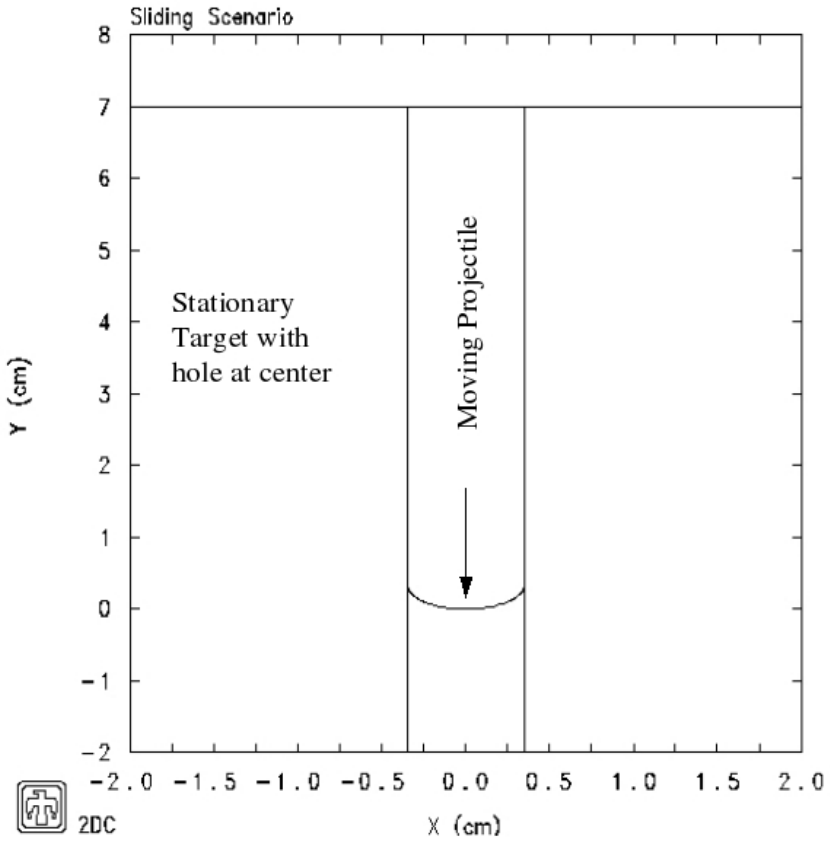

Figure 3.2 Graphic of Sliding Scenario

IV. Analysis and Results

Normal Impact Results, Part 1

The initial solutions using the normal impact model, with initial velocity of 959m/s and mesh cell size of .01cm, support the assertion that the Boundary Layer method produces more realistic solutions in the simulation of deep penetration. The maximum penetration depths for the four cases studied are presented in Table 4.1, along with the experimental result reported by Forrestal, et al [7] and the CTH result reported by Silling [13]. It should be noted that the maximum penetration depths are reached prior to 300 microseconds and the final depth computed is marginally less. The discrepancy in the maximum depth and the final position could be a result of elastic recovery in the materials or a numerical artifact. The exact penetration depth reported by Silling could not be repeated but this is most likely a result of differences in the version of CTH that was used. The current version of CTH is 6.01 while the boundary layer algorithm was implemented in version 1.027 although there is no indication of changes made to the boundary layer algorithm since its implementation. The significance of these results is that they support the assertion that the Boundary Layer method offers much improvement over the other two.

Table 4.1 Penetration Depths (.04cm Mesh)

	Experiment	Silling	Boundary Layer $\mu = .06$	Slide Line	No Slide Line	Boundary Layer $\mu = 0.$
Penetration Depth (mm)	109	115	99.1	78.2	80.5	103.6
% Difference from Experiment		+6%	-9%	-28%	-26%	-5%

Of interest also are the numerous “thermodynamic warnings” that are generated with the Slide Line method. These warnings are generated when the equation of state model calculates an unrealistic thermodynamic state for any cell, which usually manifests as a negative temperature value. The user sets an arbitrary limit for how many of these warnings can occur before the CTH calculation aborts. While there is no limit as to how high this limit can be, the accuracy of the solutions may be questionable if a significant number of these thermodynamic warnings are generated.

Pressure contour plots for these 4 cases are presented in Figures 4.1 – 4.4 with black dots indicating locations of material tracers. These tracers provide a visual indication of local material movement. At 50 microseconds, the impact events have developed enough to distinguish unique characteristics of each approach. Pressure bands of alternating intensity are visible in the projectile while a relatively smooth decreasing pressure gradient exists in the target. This is suspected to be a result of the dimensions of the model. The relatively small projectile dimensions allow pressure waves to reflect at the free surfaces and interact. The target however is large enough that pressure waves are not observed to reflect off the side and bottom free surfaces. The band of negative pressure near the target’s top free surface does indicate some boundary effect but was limited to the immediate vicinity of the surface.

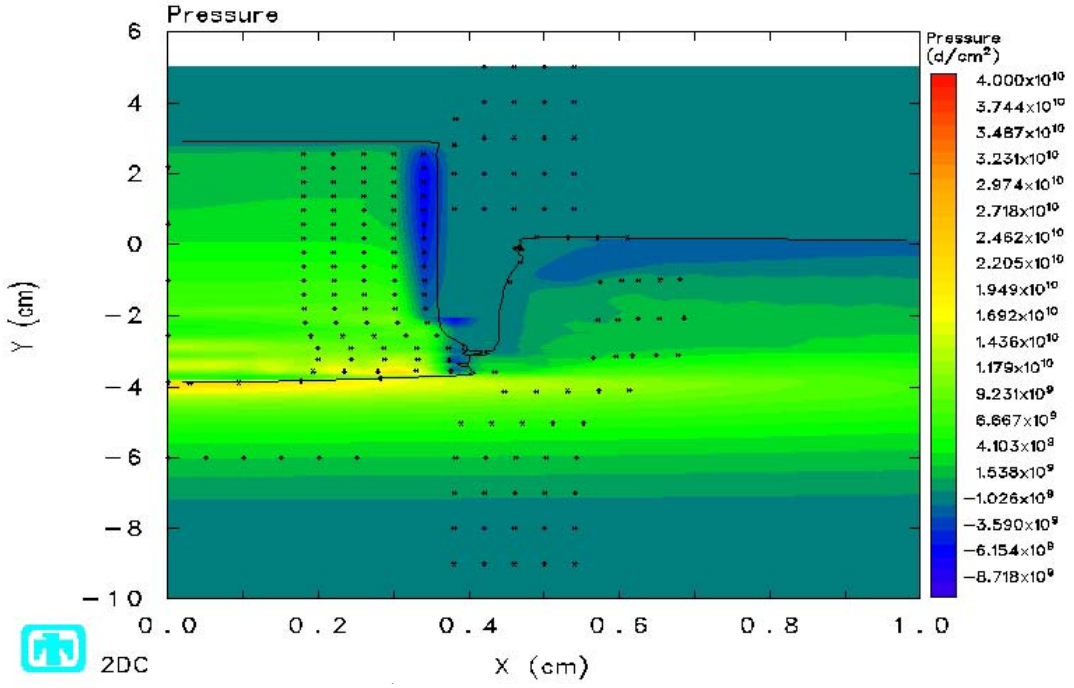

Figure 4.1 Pressure Contour at 50 µs, No Slide Line

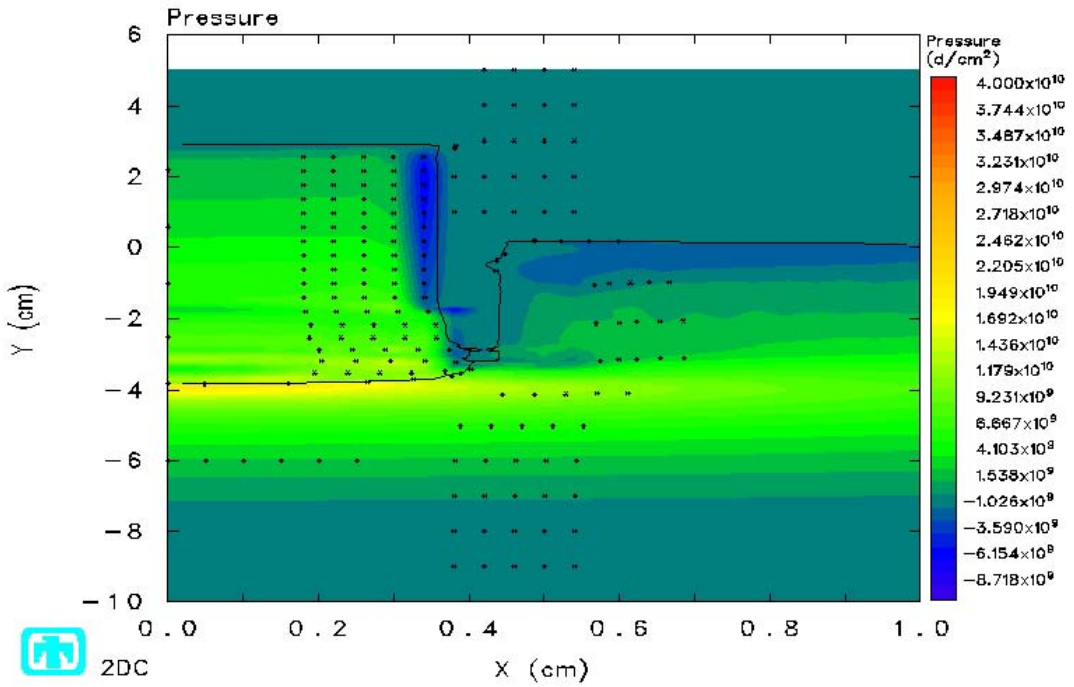

Figure 4.2 Pressure Contour at 50 µs, Slide Line

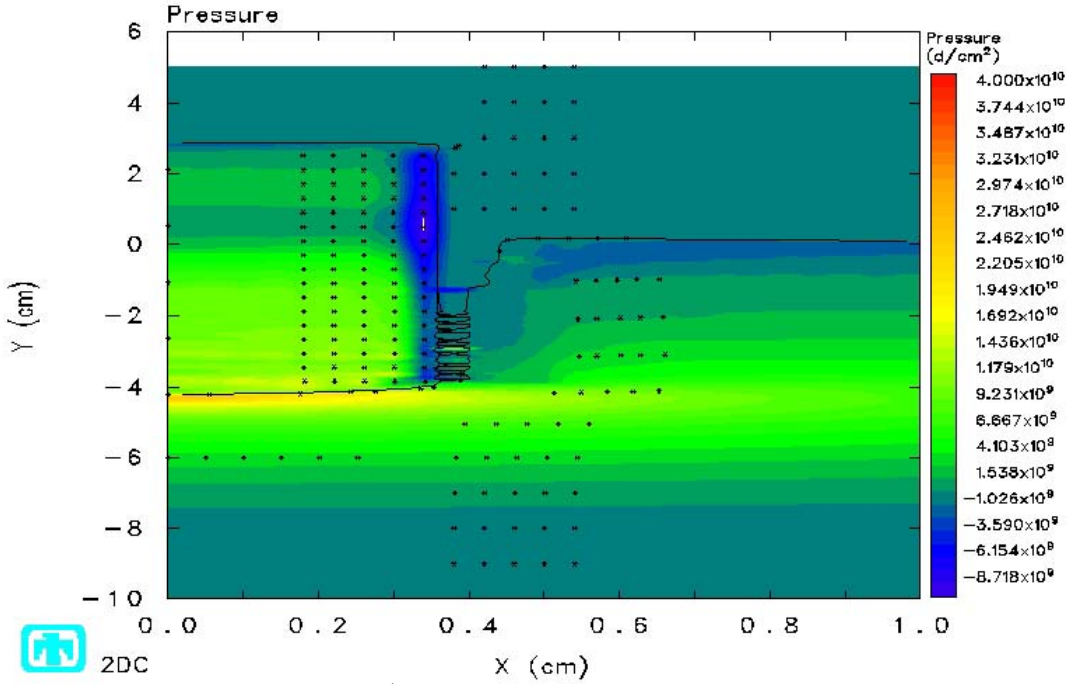

Figure 4.3 Pressure Contour at 50 µs, Boundary Layer, µ=0.06

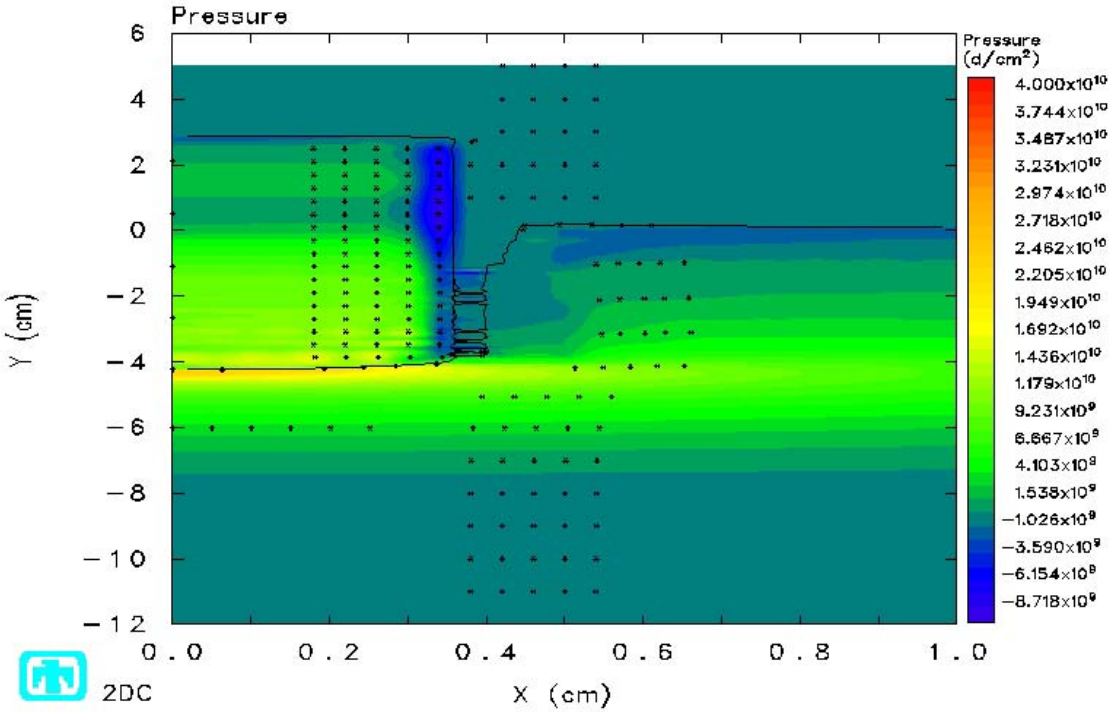

Figure 4.4 Pressure Contour at 50 µs, for Boundary Layer, µ=0.0

Additionally, these figures clearly show the extent to which preservation of the projectile shape is maintained through use of the Boundary Layer method. However, one disconcerting feature which is most prevalent with the Boundary Layer method is the existence of horizontal material bands between the projectile and the target. This can be attributed to the coarseness of the mesh which makes it more difficult for CTH to track material surfaces. Small distortions of the projectile surface can affect which cells are identified as boundary layer cells as can be seen in Figure 4.5 with the boundary layer type values defined in Table 4.2. Since the target material in mixed cells is attached to the projectile, additional target material is pulled along with the projectile whenever the hard boundary layer shifts towards the target material. The effect of the frozen slip layer compounds this issue since that material is forced to move down into the target with the projectile. This effect is expected to be reduced as mesh size is reduced but not entirely eliminated. (It should be noted that the program used to generate these plots, namely CTHPLT, applies a smoothing technique that can produce misleading results. Since these are contour plots, the program does not allow discreet jumps between the data values; all plotted data must transition smoothly. In Figure 4.5, no soft boundary layer, shown in red, actually exists in the hard projectile material; this is purely a result of smoothing.)

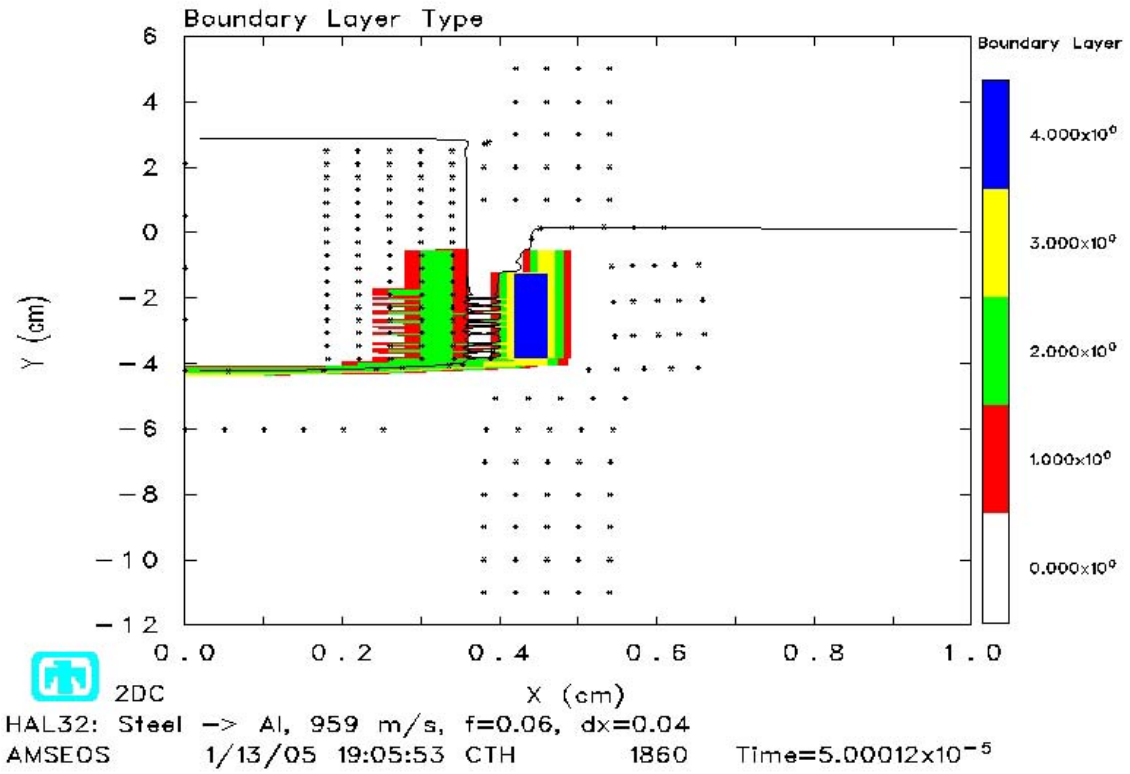

Figure 4.5 Boundary Layer Type at 50 μs, μ=0.06

Table 4.2 Boundary Layer Types

0	Cell is not in a boundary layer
1	Cell is in a soft boundary layer but not a slip layer
2	Cell is in a hard boundary layer
3	Cell is in a non-frozen slip layer
4	Cell is in a frozen slip layer

The temperature profiles are also useful in discussing the differences in these solutions and are shown in Figures 4.6 – 4.9. The No Slide Line and the Slide Line cases show similar elevated temperature profiles while the Boundary Layer cases show relatively little change in temperature. An increase in temperature can be interpreted as localized plastic deformation, since these solutions do not account for heat transfer.

Considering the significant deformation resulting from the impact event, elevated temperatures near the impact surface would be expected.

It should be noted at this point that these observations and assertions are based on a solution obtained with a relatively coarse mesh. A finer mesh is necessary before any realistic comparisons between the material interface models.

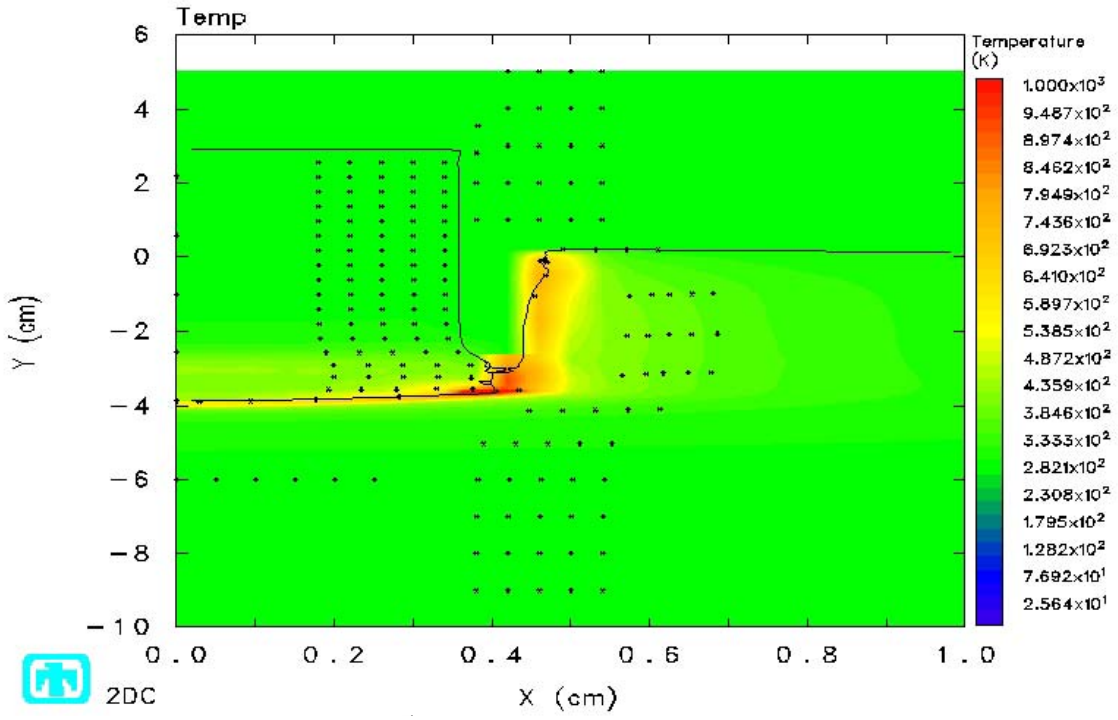

Figure 4.6 Temperature at 50 µs, No Slide Line

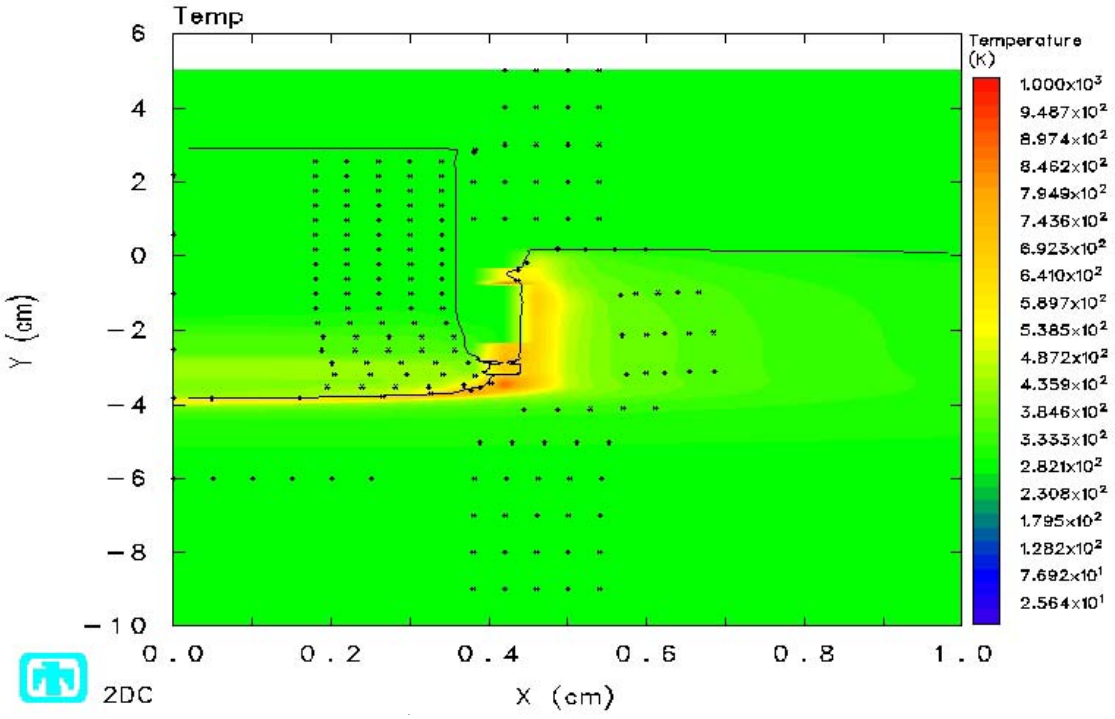

Figure 4.7 Temperature at 50 µs, Slide Line

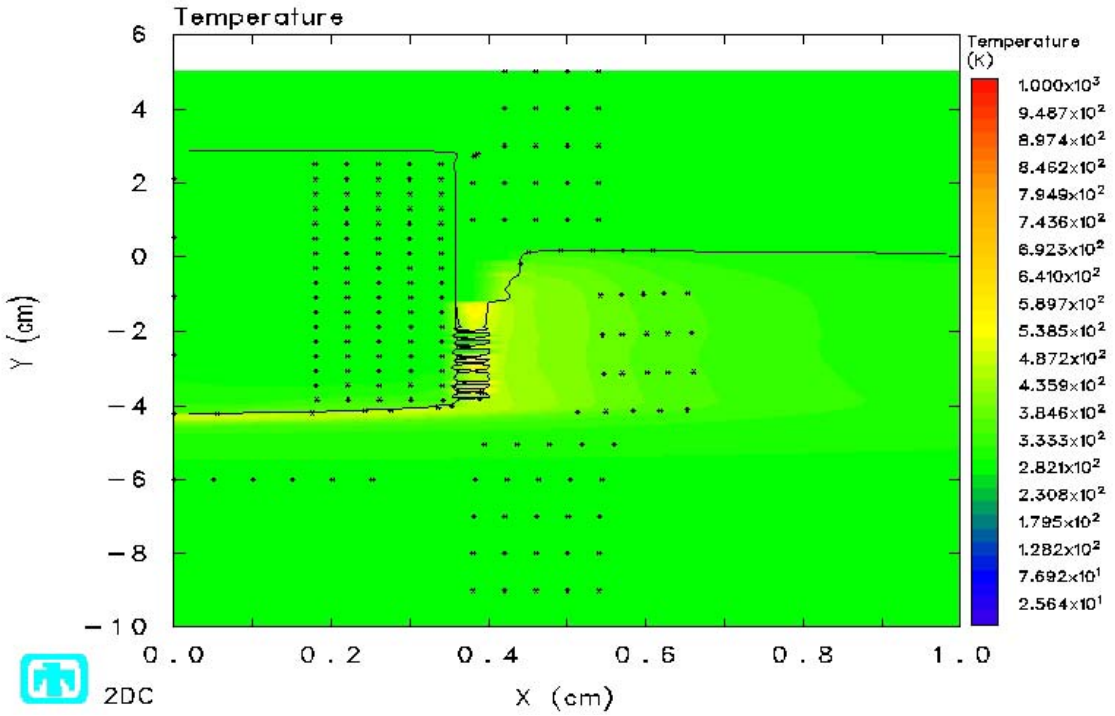

Figure 4.8 Temperature at 50 µs, Boundary Layer, µ=.06

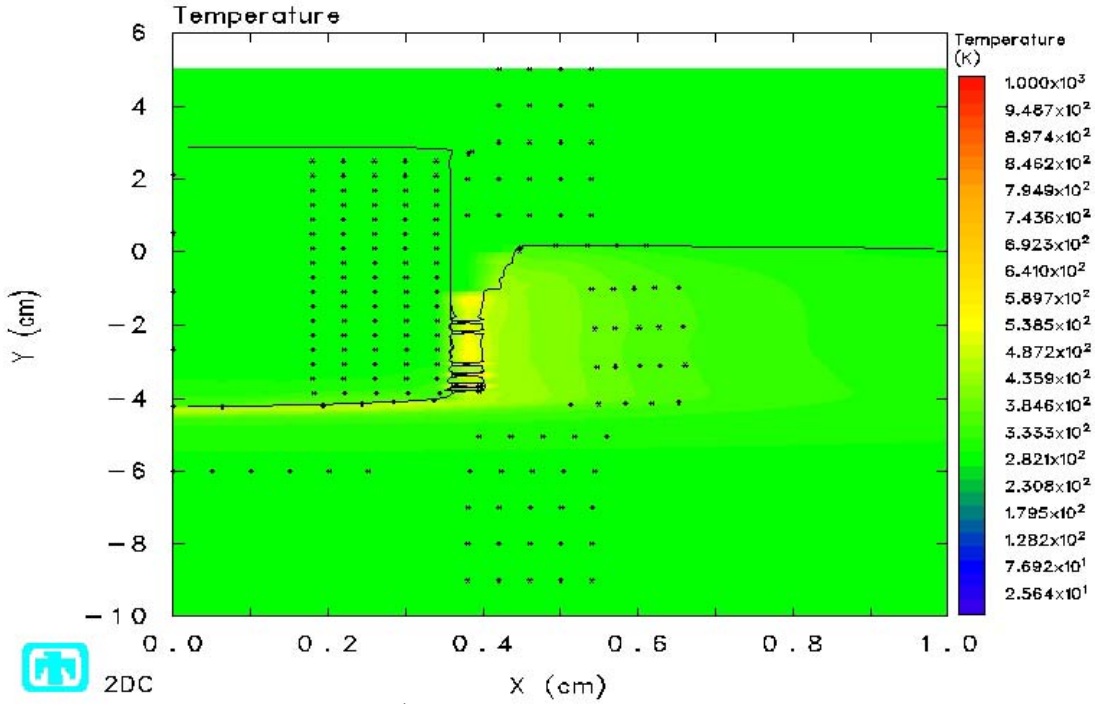

Figure 4.9 Temperature at 50 μs, Boundary Layer, μ=0.0

The second set of solutions obtained using a mesh cell size of .01cm appears to negate the assertions that were previously made with a mesh cell size of .04cm. Figures 4.10 - 4.12 again show the pressure contours for the three cases at 50 microseconds. Similar pressure bands in the projectile are present in all three cases. Perhaps the key observation made from these figures is that the shape of the penetrator does not distort noticeably in any of the three cases. The shape of the deformed target varies somewhat but the differences seen along the vertical face is most likely due to mesh coarseness affecting the material interface tracker algorithm.

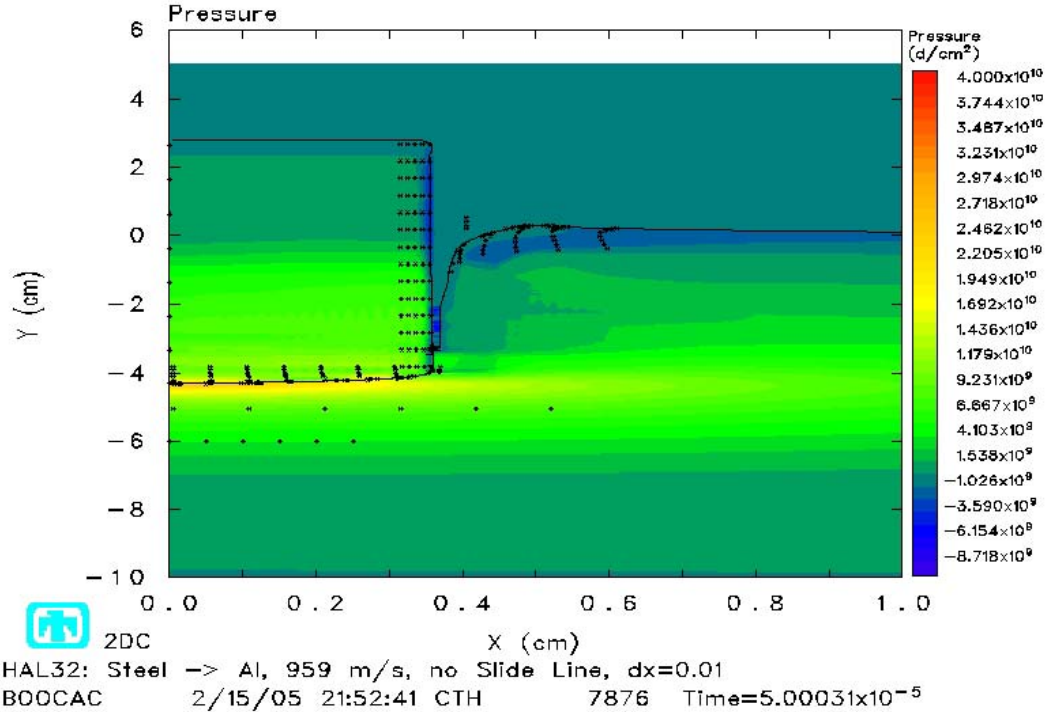

Figure 4.10 Pressure Contour at 50 µs, No Slide Line

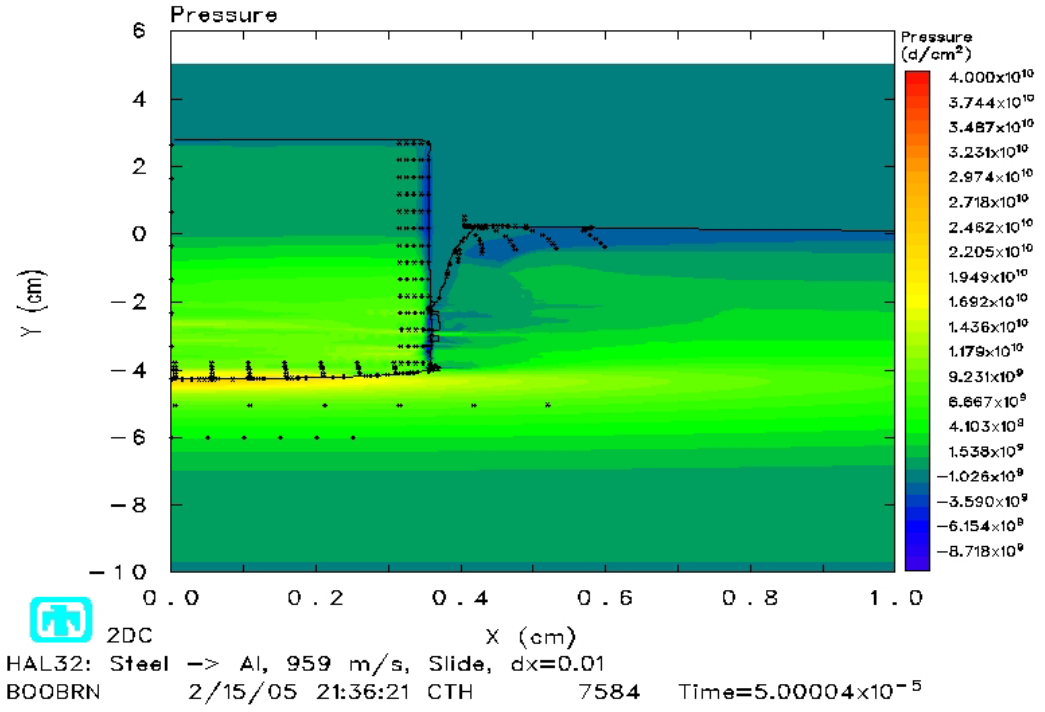

Figure 4.11 Pressure Contour at 50 µs, Slide Line

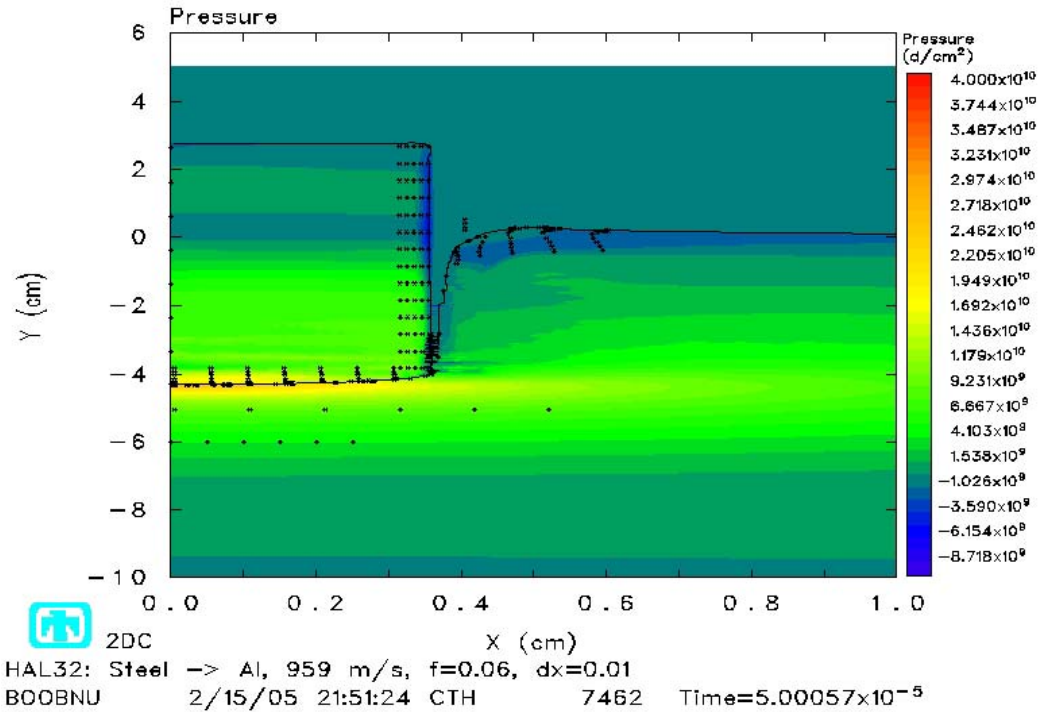

Figure 4.12 Pressure Contour at 50 μs, Boundary Layer, μ=0.06

A projectile material tracer located in the nose of the projectile, with initial coordinates x=.205 and y=.305, was selected to compare pressure, deviatoric shear stress, and normal stress histories for each method. The conditions at this tracer are representative of the overall projectile contact surface since its position relative to the projectile and the contact surface remains essentially constant, less than .002cm fluctuation. These tracer history plots are shown in Figure 4.13 – 4.15 and are virtually indistinguishable. Target material tracers were observed to displace beyond the right edge of the projectile within the first 10 microseconds due to severe plastic deformation of the target material along the contact surface. Since this places them outside the impact region, their data history would not reflect conditions which develop near the material interface for the entirety of the solution time.

The penetration depths at 50 microseconds are compared in Table 4.2. While the depth varies by up to .377cm with the .04cm mesh, the max difference is only .056cm with the .01cm mesh.

Table 4.2 Penetration Depths at 50 μs

	Boundary Layer $\mu = .06$	Slide Line	No Slide Line
.04cm mesh	4.225 cm	3.848 cm	3.890 cm
.01cm mesh	4.331 cm	4.367 cm	4.311 cm

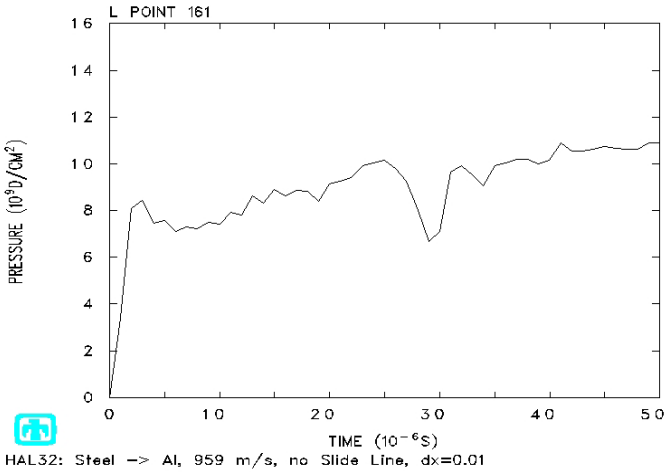

a) No Slide Line

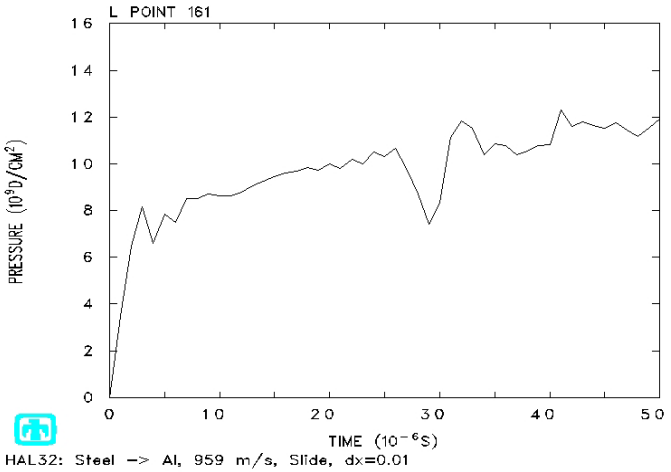

b) Slide Line

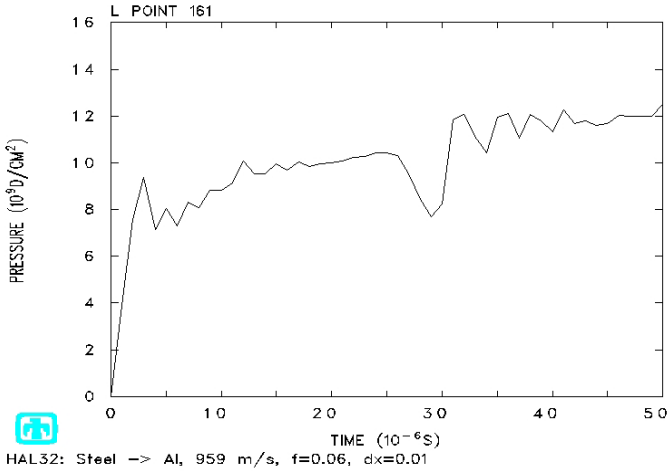

c) Boundary Layer

Figure 4.13 Projectile Surface Pressure History

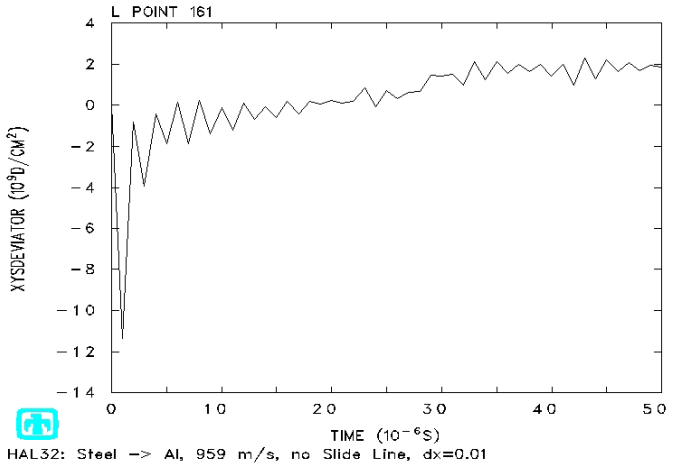

a) No Slide Line

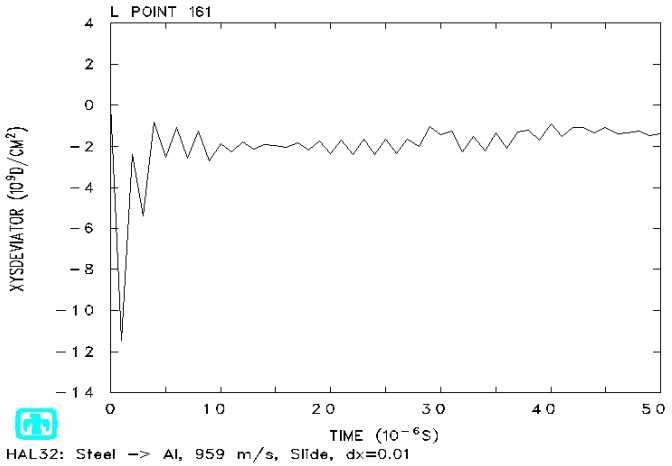

b) Slide Line

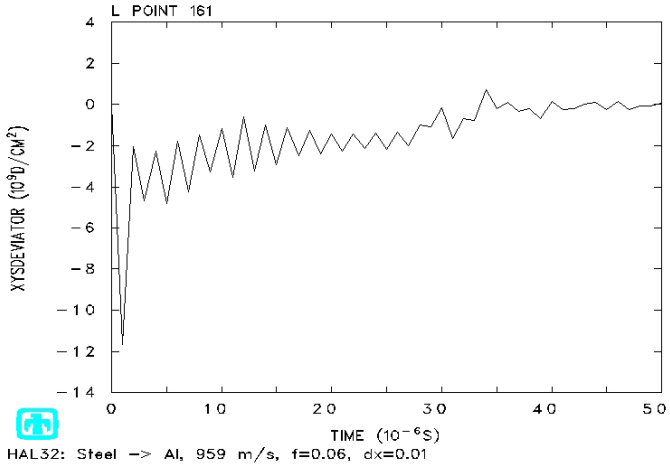

c) Boundary Layer

Figure 4.14 Projectile Surface Deviatoric Shear Stress History

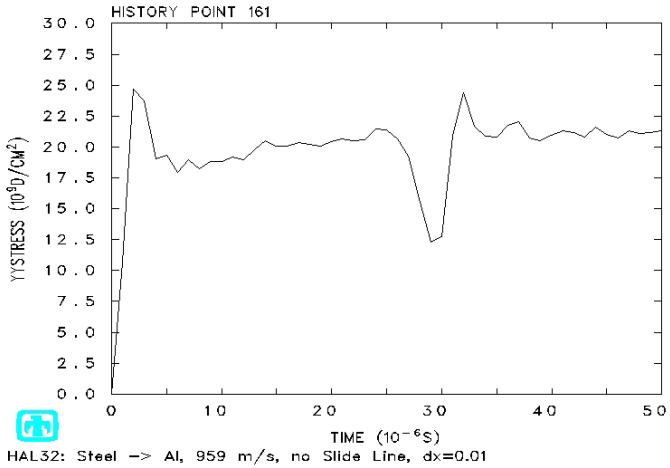

a) No Slide Line

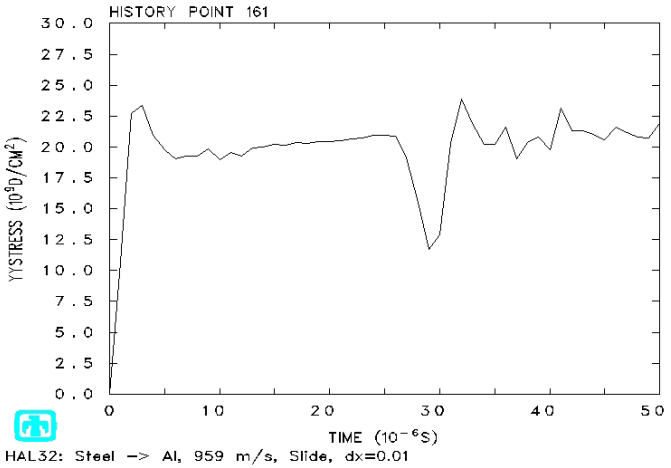

b) Slide Line

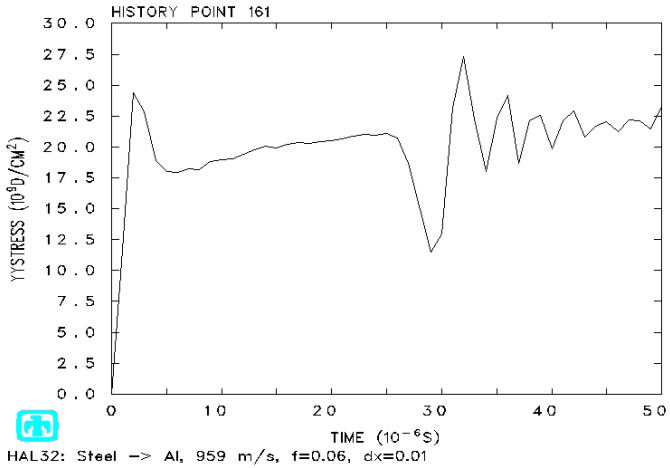

c) Boundary Layer

Figure 4.15 Projectile Surface Normal Stress History

These results suggest that as the size of mesh cells decrease, the differences in solutions obtained with the three methods for defining material interfaces become negligible. Using the Boundary Layer method to preserve the shape of the penetrator does not appear to be necessary. At this level of mesh refinement, the effect of numerical erosion of the penetrator surface is not a significant factor. The only apparent advantage to using the Boundary Layer method is the capability to explicitly add friction to the solution except that in the current scenario, where our solution is underestimating the maximum penetration depth, adding friction results in a solution even further from the experimentally measured depth. This method doesn't even appear to be advantageous for the problem of penetration and perforation for which it was developed. However, if one considers that the boundary layer algorithm was developed in 1992 and that the deep penetration model used to validate it was only refined to a .04 cm mesh, the need for this method becomes almost apparent. Given the level of computing capability present in 1992, the computational requirements to obtain solutions for a .01cm mesh versus a .04cm mesh were most likely time and cost prohibitive. Even with the modern computers available in the AFIT/ENY lab, a full solution out to 300 microseconds was not feasible. The benefits of the Boundary Layer method then would appear to only apply for relatively coarse meshes. However, it would be premature to discard this technique as a viable option based on the limited results obtained to this point.

A comparison of the temperature profiles shown in Figures 4.16 - 4.18 indicates a difference in the solutions that may be significant. While the total area of increased temperature is comparable, the temperature magnitudes are not. The magnitude of the

temperature increase and associated plasticity is lower for the Boundary Layer method as observed previously for the .04 cm mesh solutions. Also, since the projectile shows virtually no deformation, the plasticity is isolated to the target material. Considering the differences in material properties for the steel projectile and the aluminum target, this is not a surprising result.

These test cases have served to provide some insight concerning the effects of the three methods for defining material interfaces but a scenario with more material interaction is necessary to obtain any more useful observations. Since previous gouging simulations using the real materials have shown that significant material interaction occurs under the right conditions, the next phase of this research examines an impact scenario with real materials.

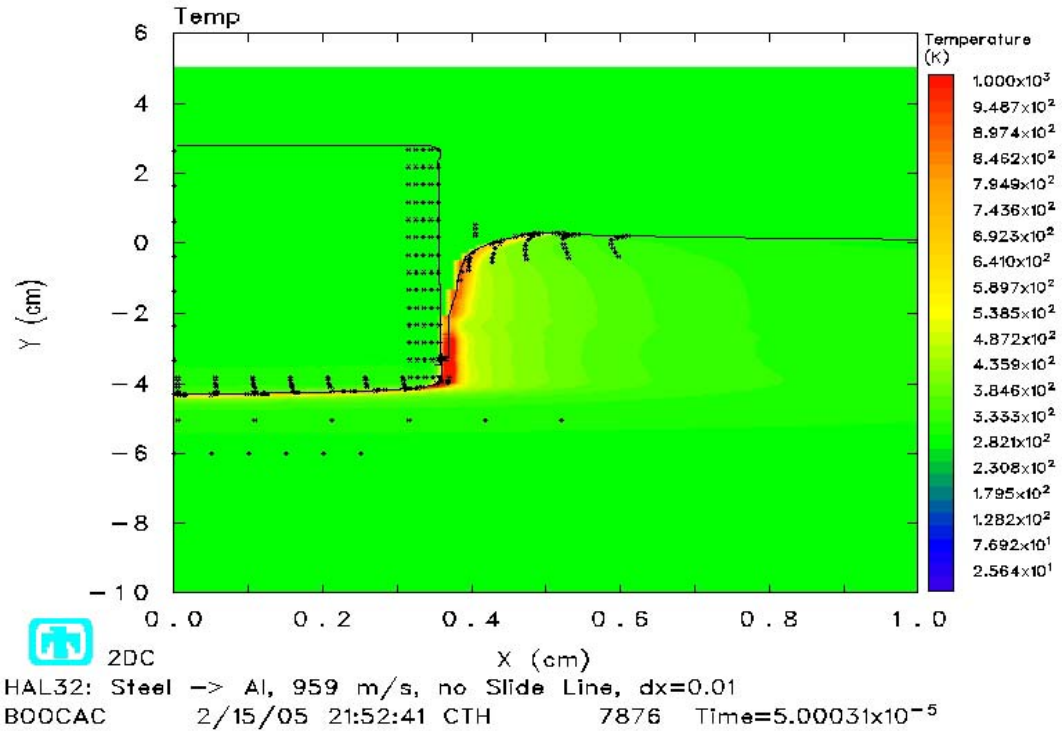

Figure 4.16 Temperature at 50 μs, No Slide Line

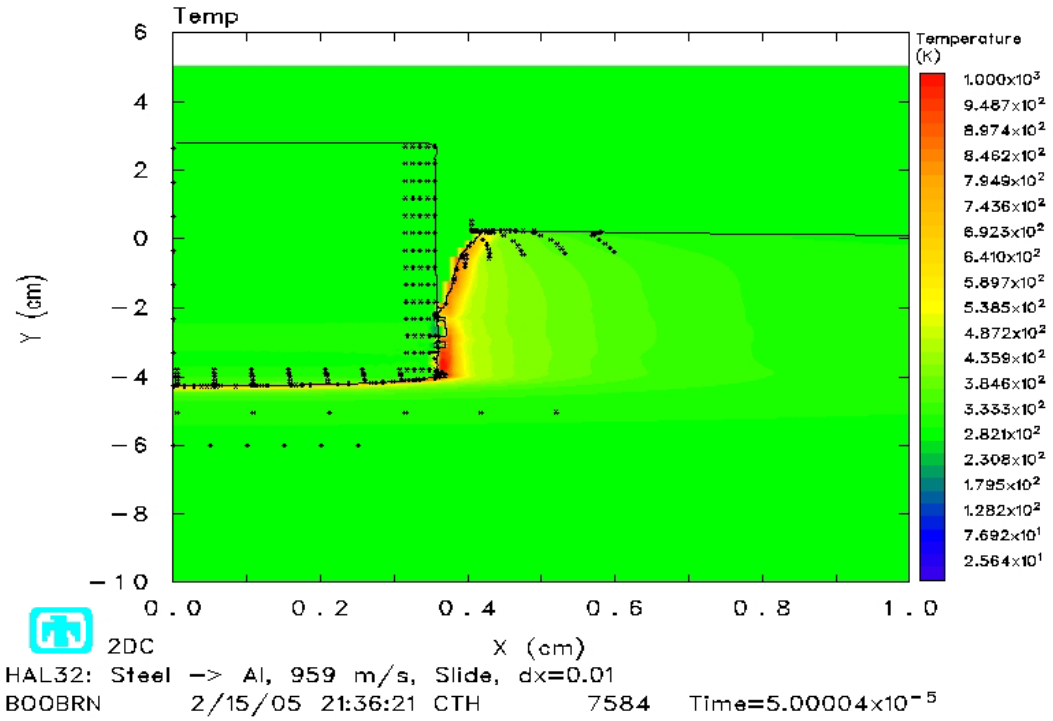

Figure 4.17 Temperature at 50 µs, Slide Line

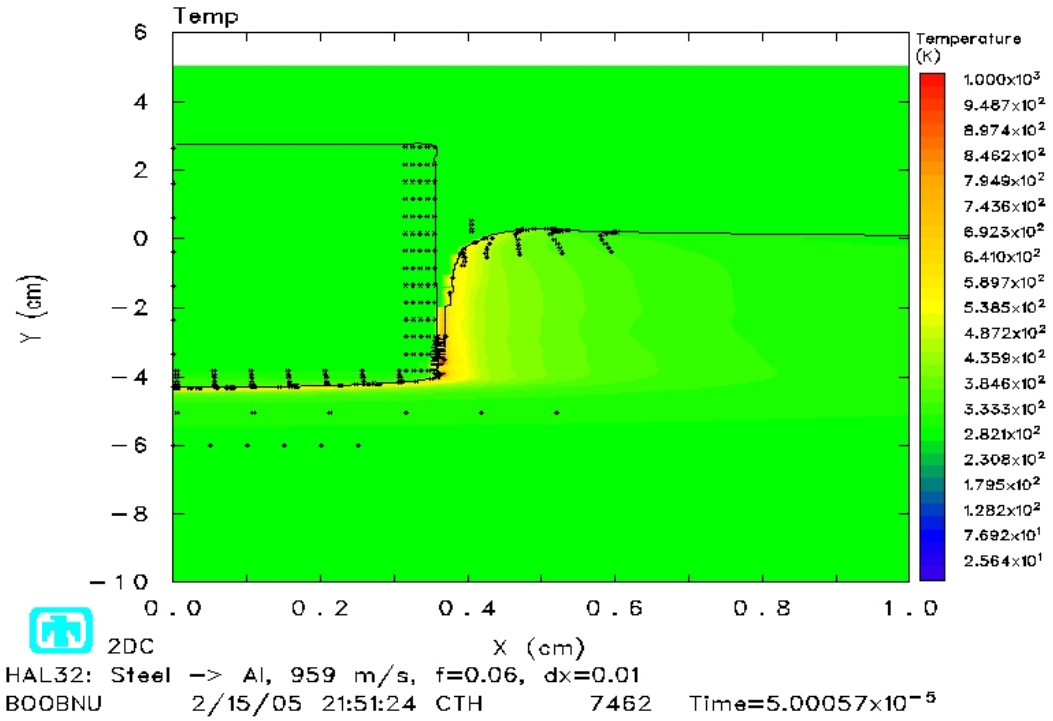

Figure 4.18 Temperature at 50 µs, Boundary Layer

Before proceeding however, the issue alluded to previously of the horizontal material bands between the vertical surfaces of the projectile and the target was given more consideration. At a mesh cell size of .01cm, these material bands are still present in the Boundary Layer case as can be seen in the pressure and temperature contours above. The assertion made previously was that the formation of these bands is a product of mesh coarseness and the adverse effect it has on accurately defining boundary layers. The amount of material banding was reduced from the .04cm mesh to the .01cm mesh but still readily visible. The mesh was refined one more time to .005cm to observe whether this banding could be reduced further. The pressure contour at 50 microseconds is shown in Figure 4.19 for the .005cm mesh to allow comparison with the previous data. The amount of material banding is slightly reduced again but still readily apparent. To refine the mesh any further would require considerable computational time that is not currently feasible since the Boundary Layer method is limited to single processor computing.

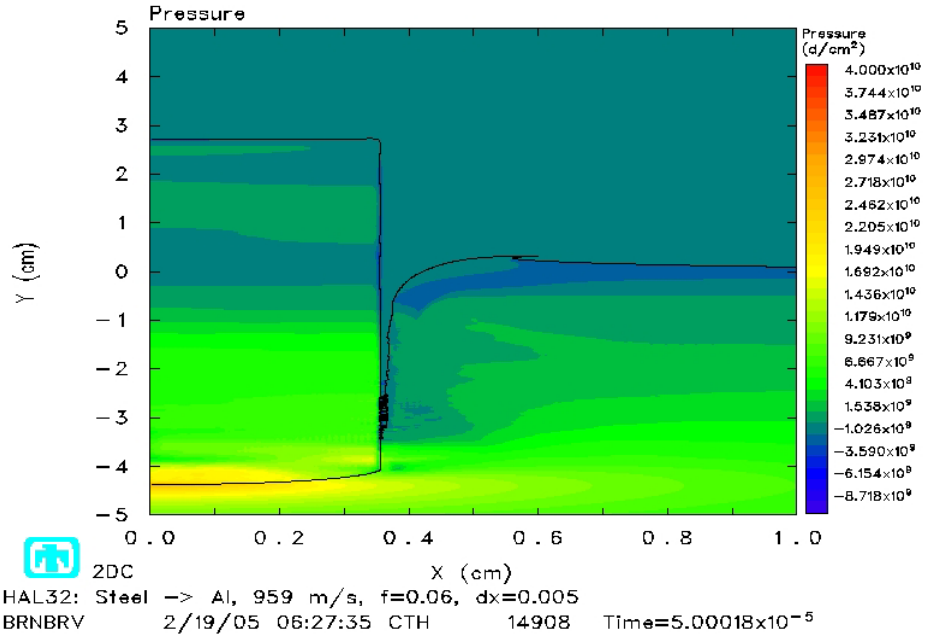

Figure 4.19 Pressure at 50 µs, .005cm Mesh, Boundary Layer

Normal Impact Results, Part 2

The results obtained for a normal impact at 1 km/s with a Vascomax 300 projectile and a 1080 Steel target reveal an event that is highly dominated by plastic deformation. Pressures near the impact surface exceed 2 GPa, the uniaxial compressive yield stress of the harder projectile material. The impact sequence for the No Slide Line case is shown in Figures 4.20 and 4.21 by way of pressure contours at 10 μs intervals. The limited penetration and severe deformation of the projectile is attributed to the similarity of the material properties which result in similar material responses. However, greater deformation is observed in the target material since the yield strength is just over 1/3 that of the projectile. By 80 μs, as it comes to rest, the amount of projectile deformation is quite extensive. There is also an extensive zone of negative pressure that has developed in the projectile. Just visible at 10 μs is a band of high pressure that develops in the projectile which increases in size and magnitude. This high pressure band propagates towards the top of the projectile as the projectile continues to deform and mushroom radially outwards. The formation of the negative pressure region begins at approximately 50 μs, just below the high pressure band, and expands as the high pressure band propagates upwards. It is hypothesized that the negative pressure region forms due to a pressure release effect cause by the propagation of the high pressure band combined with an amplified elastic response due to the similarity of the two materials involved. The fact that this negative pressure region is most extensive in the No Slide Line case supports the hypothesis that some material coupling effect is occurring. Whether this level of plastic deformation would be observed in an experimental impact

test is highly questionable. This extensive plastic deformation is most likely a purely numerical construct, since a fracture criteria was not included in these simulations.

Similar deformation is observed for the Slide Line and Boundary Layer cases as seen in Figures 4.22 – 4.25. The only significant difference observed between the three cases is the rate at which the nose of the projectiles mushrooms. The deformation of the projectile for the Boundary Layer case appears to develop at the slowest rate. This is most visible at 30 μs where a gap exists between the advancing front of the projectile material and the trailing face of the deformed target material. However, this gap does not persist as the projectile continues to mushroom and reestablish contact with the target material. In all three cases, the projectile is observed to contact the target as the impact event comes to an end. The difference in deformation rate is also evident at 60 μs by comparing the deformed height of the projectile. While the penetration depth is essentially identical, the undeformed aft end of the projectile is right at the 2cm mark in the Boundary Layer case, while it is clearly below the 2cm mark in the other two cases. These two observations suggest that the boundary layer algorithm is artificially increasing the yield stress of the projectile. Since it was implemented to preserve the penetrator shape in low velocity impacts, perhaps that effect is appearing in this case inappropriately. Perhaps this technique is not appropriate for use when the projectile is known to undergo substantial deformation.

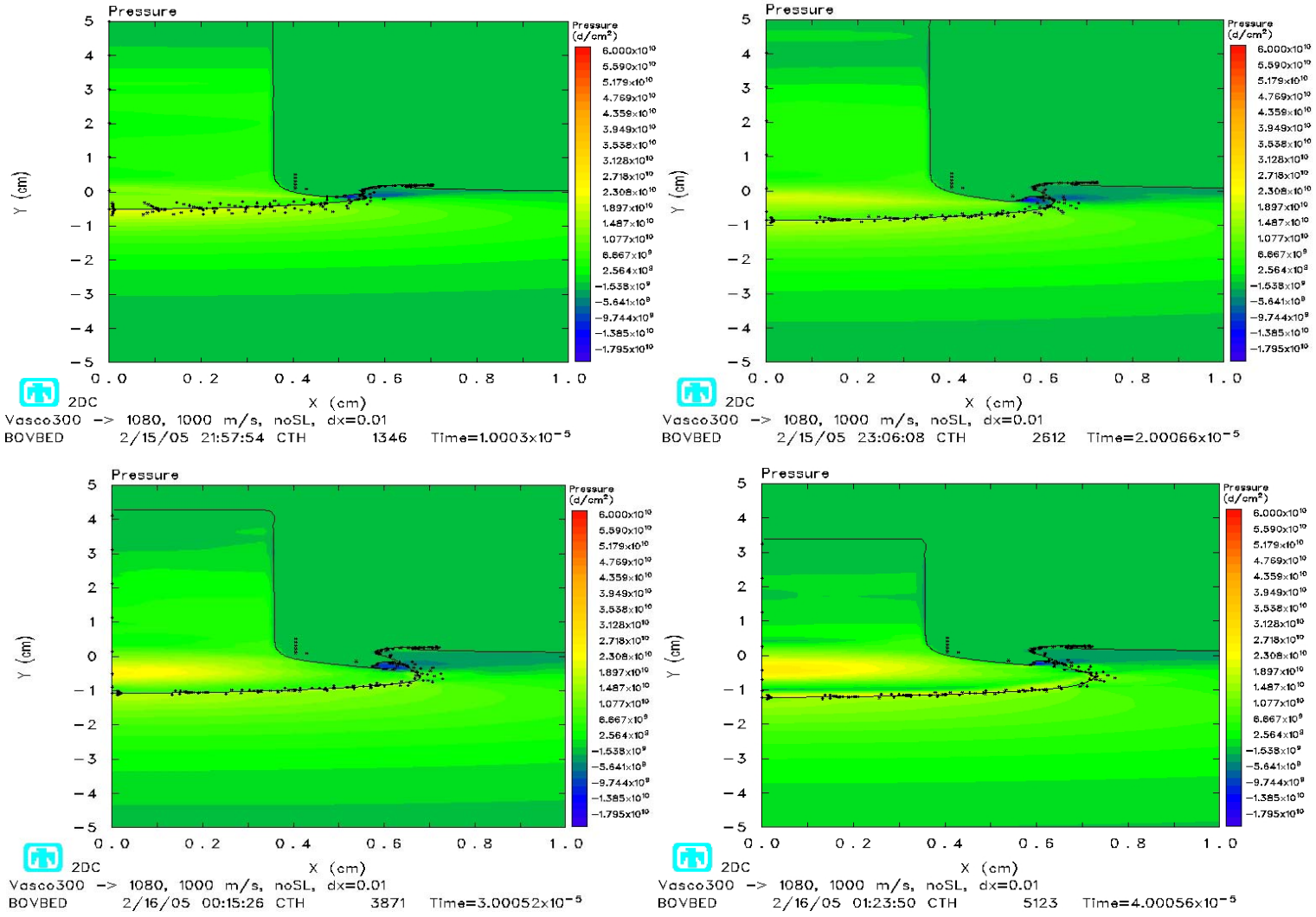

Figure 4.20 Pressure Contours at 10, 20, 30, and 40 µs, No Slide Line

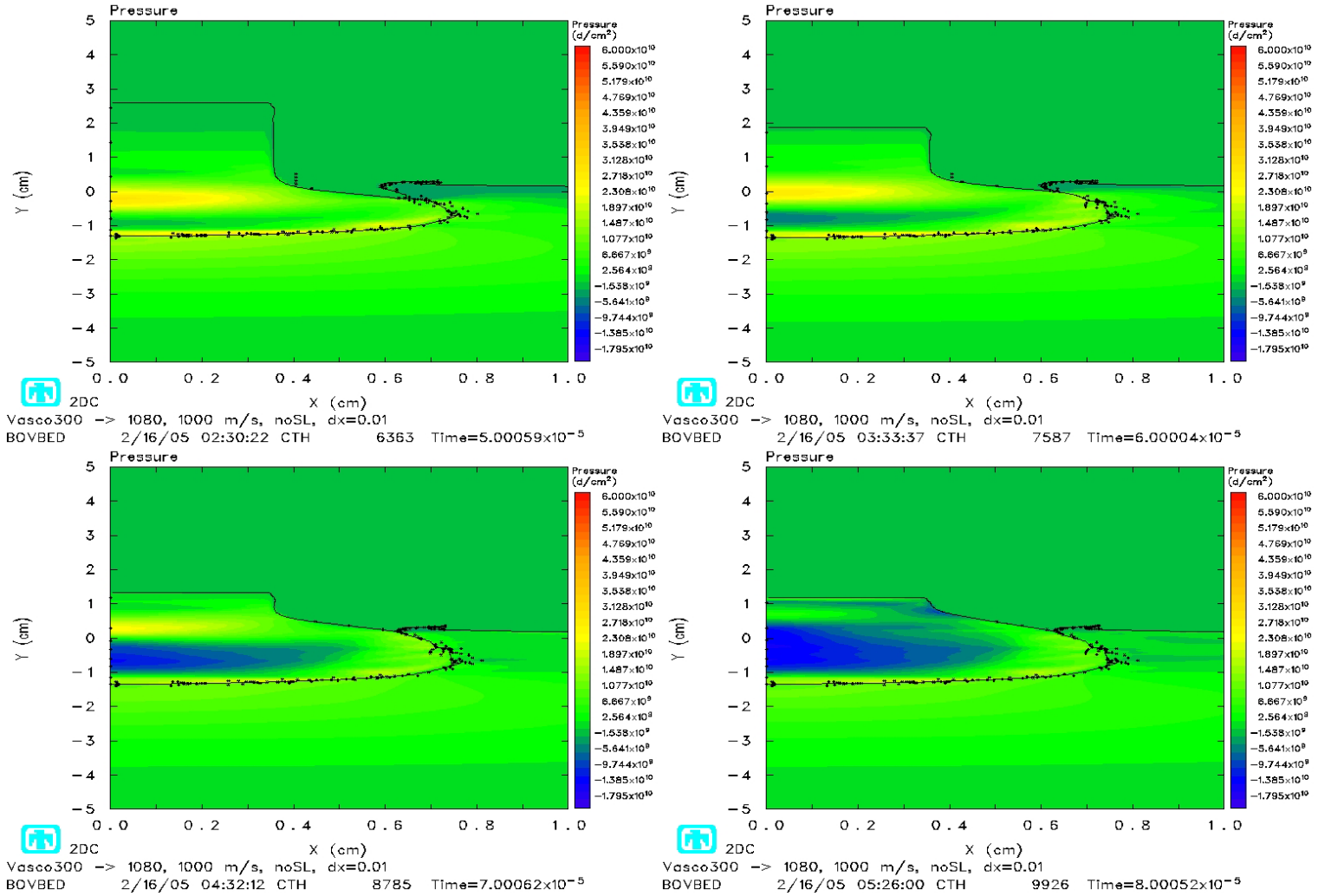

Figure 4.21 Pressure Contours at 50, 60, 70, and 80 µs, No Slide Line

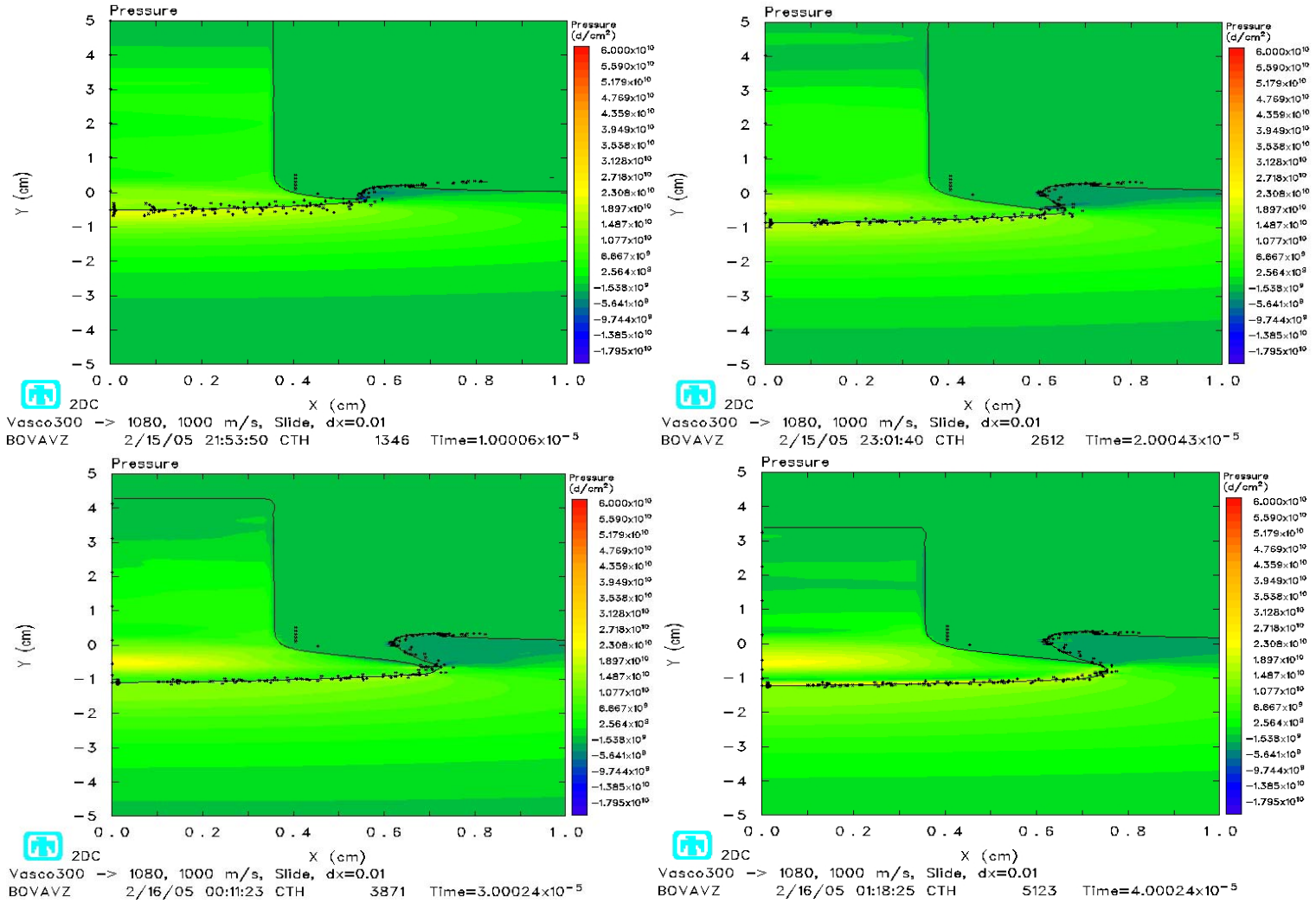

Figure 4.22 Pressure Contours at 10, 20, 30, and 40 µs, Slide Line

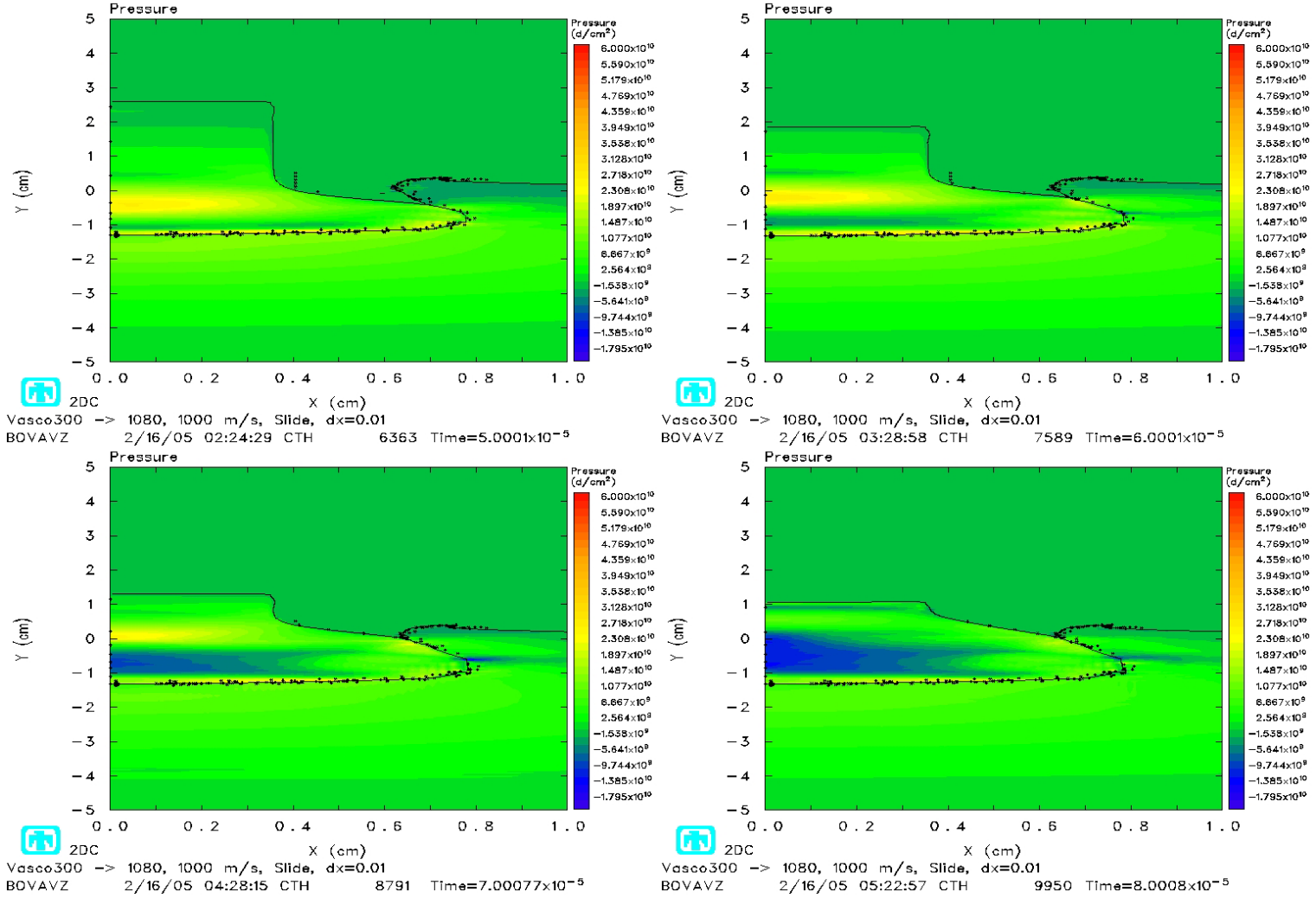

Figure 4.23 Pressure Contours at 50, 60, 70, and 80 µs, Slide Line

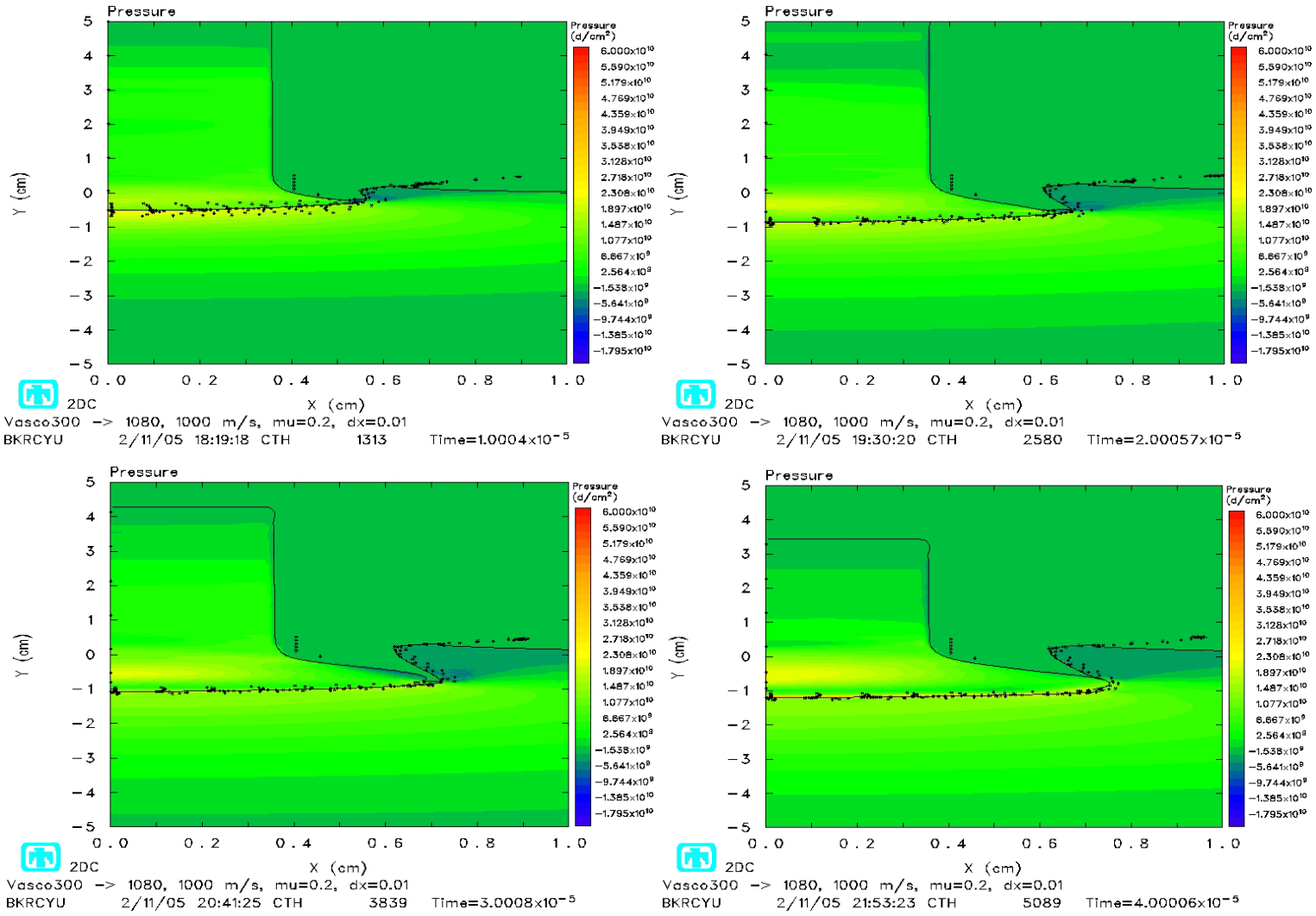

Figure 4.24 Pressure Contours at 10, 20, 30, and 40 µs, Boundary Layer

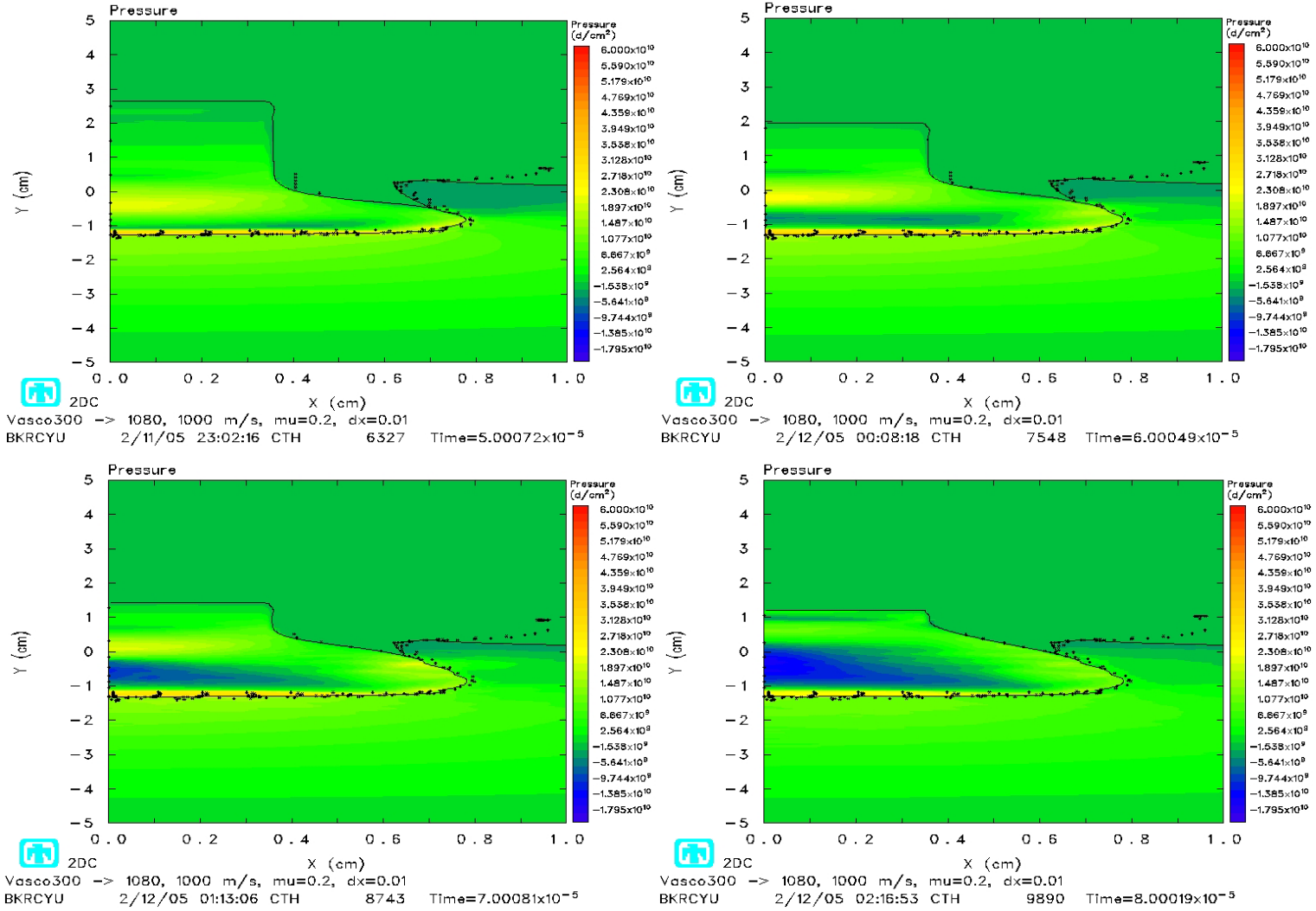

Figure 4.25 Pressure Contours at 50, 60, 70, and 80 µs, Boundary Layer

The assertion that the extensive deformation of both projectile and target material is primarily plastic deformation is supported by the temperature profiles shown in Figures 4.26 – 4.28. The temperature rise in the majority of the deformed material never reaches the melting temperatures of 1650 K for the projectile and 1835 K for the target. The No Slide Line case does show a high temperature zone along the entire contact surface of the projectile which is not present in the other cases. This is consistent with the restriction imposed by this technique that the materials are joined at the contact surface. The same level of plastic strain in the cells at the contact surface would result in a higher temperature in the projectile material due to its higher yield strength. Consideration of friction mechanisms identified by Bayer[3] would suggest that the No Slide Line technique simulates the extreme scenario of pure adhesion along perfectly smooth surfaces with 100% contact. Likewise, the Boundary Layer technique is simulating adhesion along surfaces with less than 100% contact; while the Slide Line technique as intended is simulating frictionless sliding to the extent possible considering numerical artifacts may be a factor.

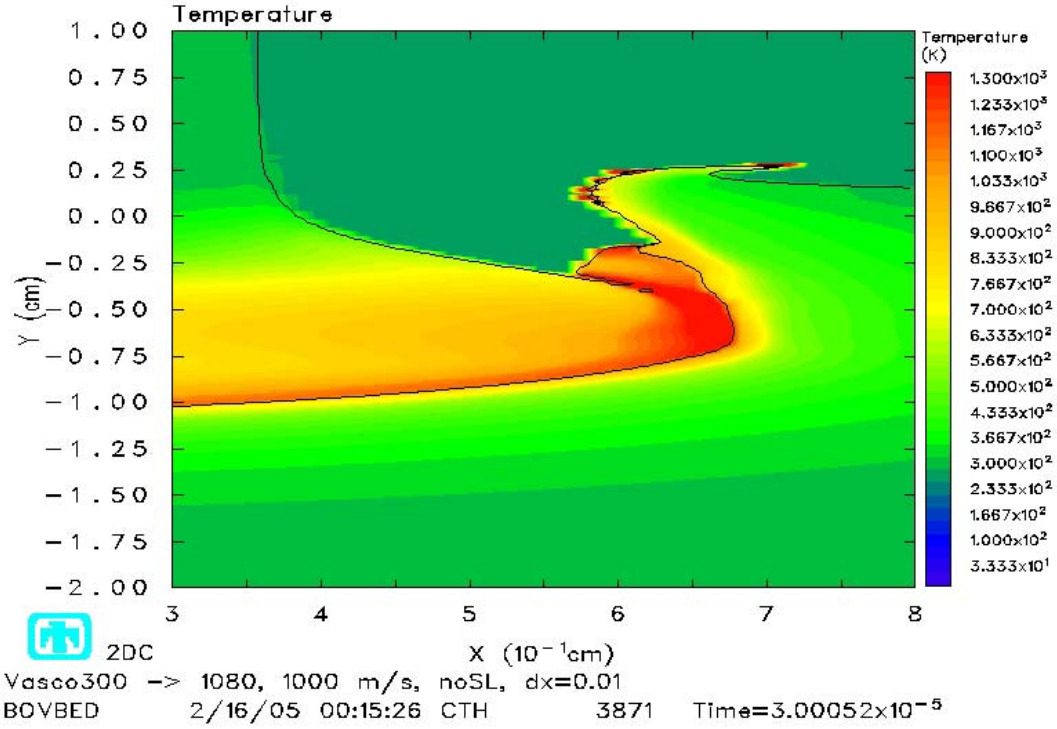

Figure 4.26 Temperature at 30 µs, No Slide Line

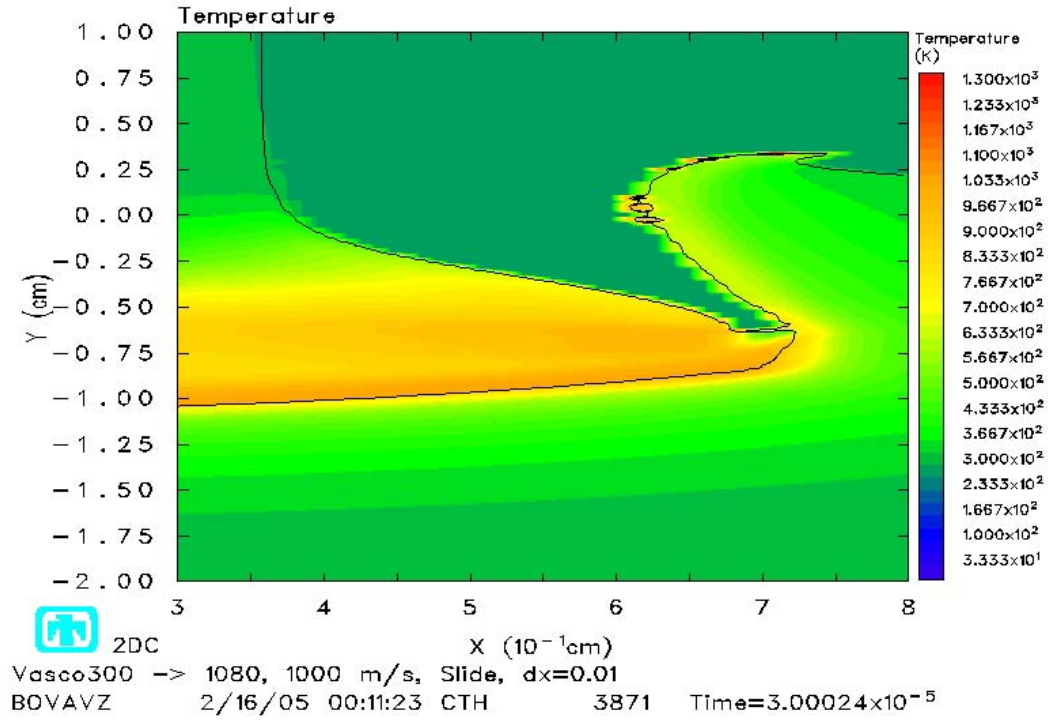

Figure 4.27 Temperature at 30 µs, Slide Line

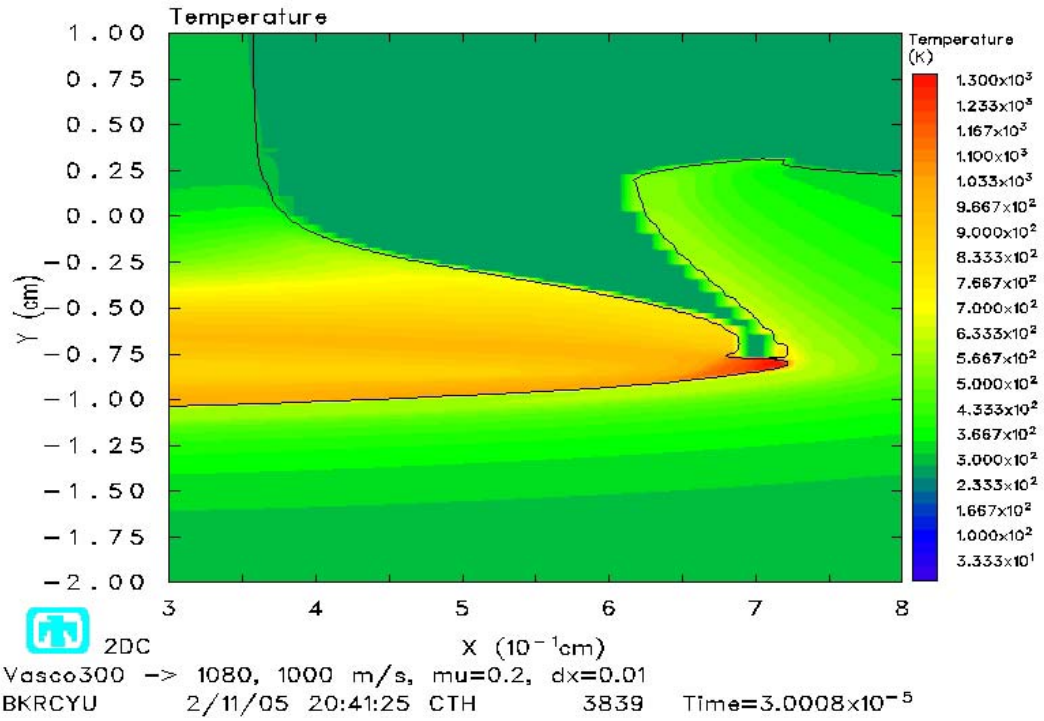

Figure 4.28 Temperature at 30 µs, Boundary Layer

To confirm the similarities between the three material interface methods that have been observed on a global scale, two projectile material tracers were selected to evaluate the conditions in the projectile near the contact surface. These two tracers are numbered 86, with initial coordinates x=.205 and y=.305, and 107 with initial coordinates x=.355 and y=.505. Tracer 86 is representative of the area near the center of the projectile nose while tracer 107 is representative of the area near the outer edge of the nose which sees the greatest deformation. These tracers are located near enough to the contact surface to evaluate the influence of the different material interface methods on the solution but far enough to not be directly involved in the unique numerical processes employed by each method.

Before discussing these figures, the issue of thermodynamic warnings mentioned previously needs to be addressed again. The solution obtained with the Slide Line method automatically aborted at approximately 95 μs due to the excessive number of thermodynamic warnings, exceeding the arbitrary limit of one million. There is a note in the CTH reference manual that suggests caution when using the Slide Line method since it can generate unexpected results. With this in mind the results presented for the Slide Line method should be viewed with some concern for their accuracy.

The displacement history of tracer 86 (Figure 4.29) shows a similar response pattern for all three methods but a significant difference in magnitude. The largest final displacement is observed with the No Slide Line method (.37cm), followed by the Slide Line method (.32cm), and the least displacement is observed with the Boundary Layer method (.22cm). This supports the earlier observation that less plastic deformation occurs with the Boundary Layer method. The largest difference in final displacement is about .15cm or 40% of the largest displacement observed. A small recovery is also evident once the maximum displacement has been reach with the Slide Line and Boundary Layer methods.

Similar observations can be made regarding the temperature history of tracer 86 (Figure 4.30). The percent difference in temperature increase is not as large however across the three methods. The difference of about 125K is only 15% of the maximum temperature increase.

The pressure history of tracer 86 (Figure 4.31) indicates an initial spike in pressure due to the initial impact which relaxes until another pressure rise is observed at

40 μs. While the initial spike has a similar magnitude of about 2GPa across all three methods, the magnitude resulting from the second pressure rise varies. The peak magnitude of this second pressure rise is approximately 2GPa for the No Slide Line method, 3GPa for the Slide Line method and 3.3GPa for the Boundary Layer method. This second pressure rise is possibly due to a pressure wave generated due to the initial impact which has propagated thru the projectile and reflected back from the free surface at the tail end. The significant differences in the magnitude of this reflected pressure wave is unexpected.

The deviatoric shear stress history of tracer 86 (Figure 4.32) also shows similar responses for all three methods. An initial negative shear spike of about -900MPa due to the impact is observed followed by a rapid increase in shear to an equally large positive value. The positive shear is sustained until approximately 30 μs, when the shear values rapidly drop and remain negative for the remainder of the solution time. This drop results in shear magnitudes less than half that of the initial spike for the Boundary Layer method while the drop is more severe for the other two methods and is approximately the same magnitude as the initial spike. This pattern of shear stress development could be a result of the differences in the yield stress and plastic deformation rates of the two materials. A shear response would be expected if the materials which are in contact are deforming at different rates.

The y-component of normal stress for tracer 86 (Figure 4.33) shows significant time response differences for the three methods from 10 to 60 μs. With the No Slide Line method the response is almost identical to the pressure response shown in Figure 4.31. A

slight rise is evident with the Slide Line method that follows the pressure response but not to the extent of the No Slide Line method. The Boundary Layer method shows relatively little change during this time interval. After 60 μs, the Slide Line method and the Boundary Layer method show a steady drop toward zero stress while the No Slide Line method only drops to about 1GPa.

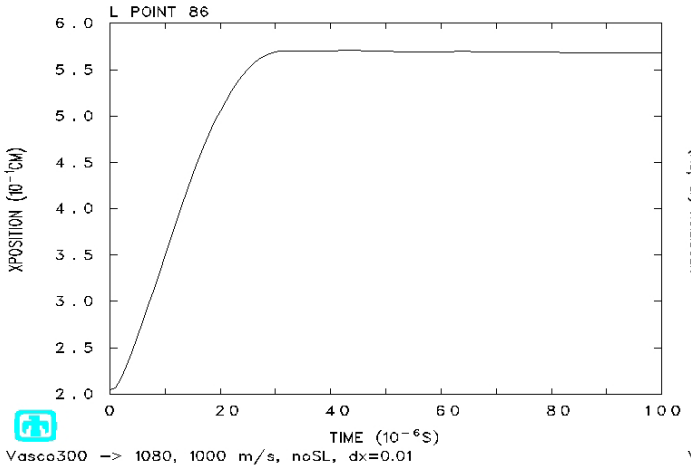

a) No Slide Line

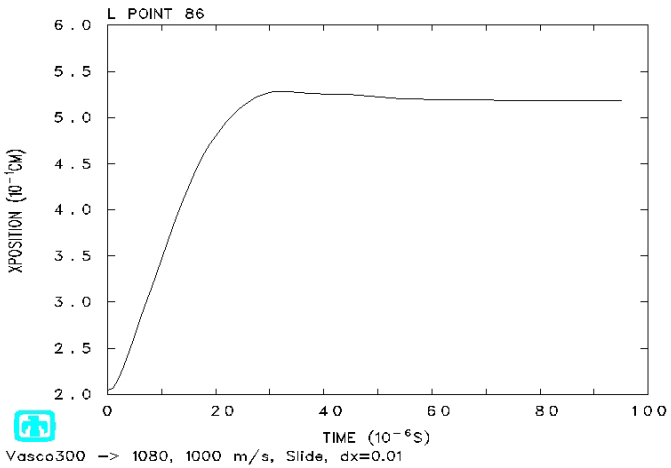

b) Slide Line

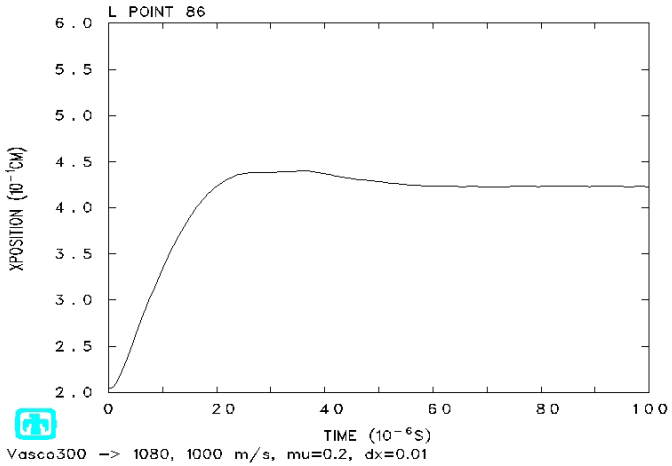

c) Boundary Layer

Figure 4.29 Tracer 86, x-Coordinate History

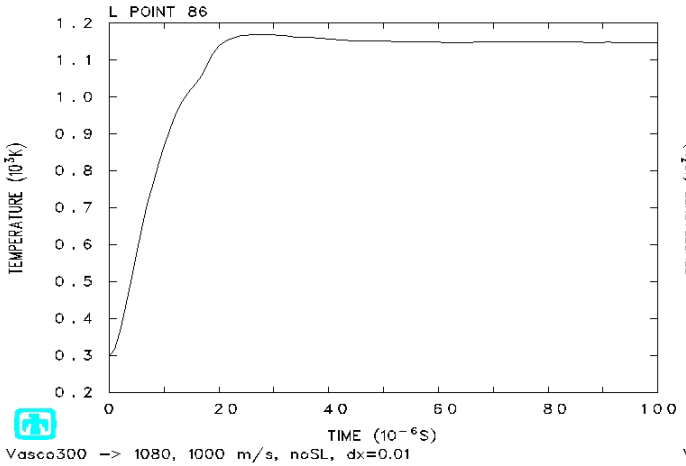

a) No Slide Line

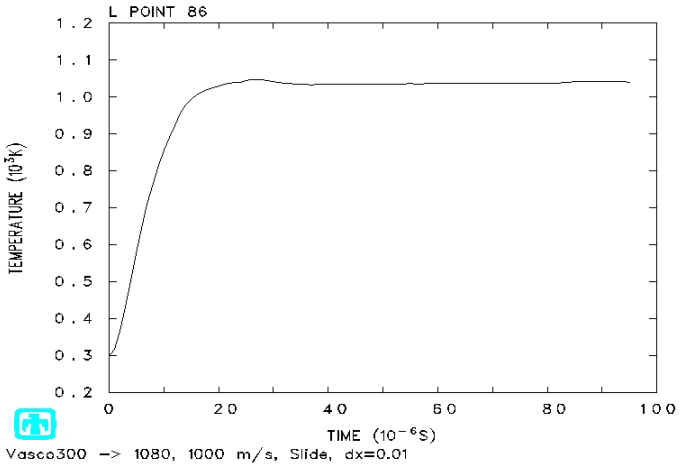

b) Slide Line

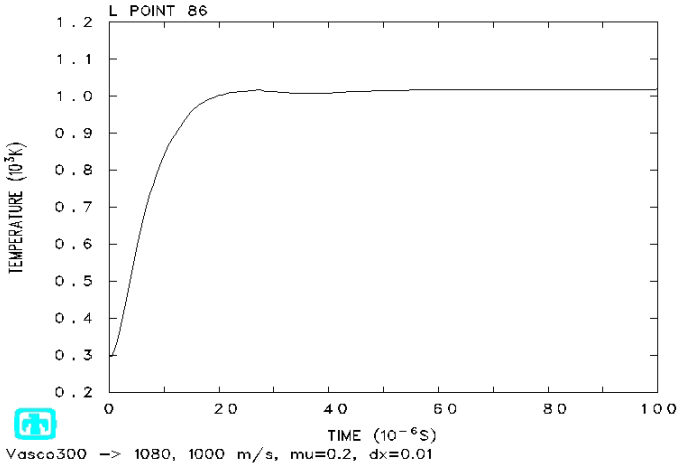

c) Boundary Layer

Figure 4.30 Tracer 86, Temperature History

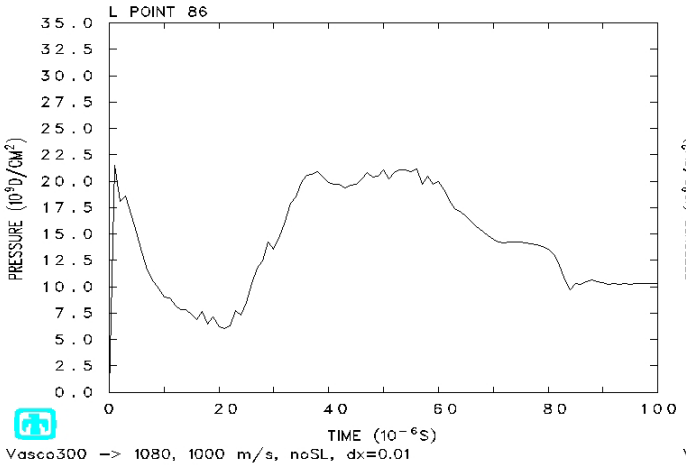

a) No Slide Line

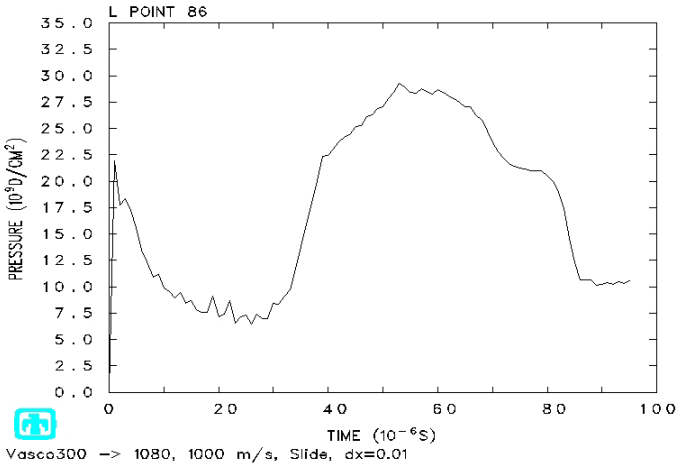

b) Slide Line

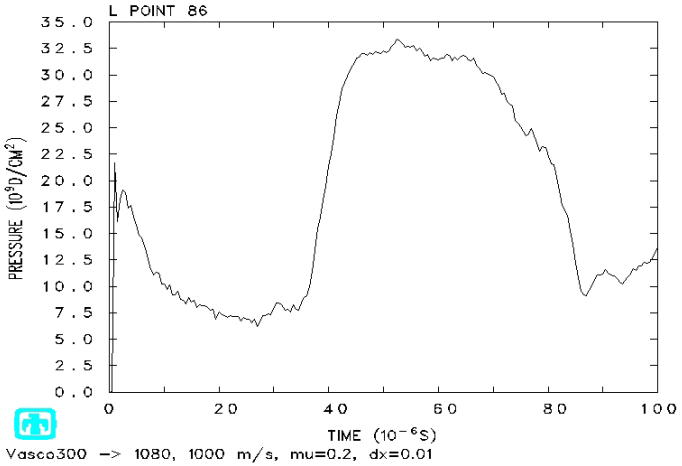

c) Boundary Layer

Figure 4.31 Tracer 86, Pressure History

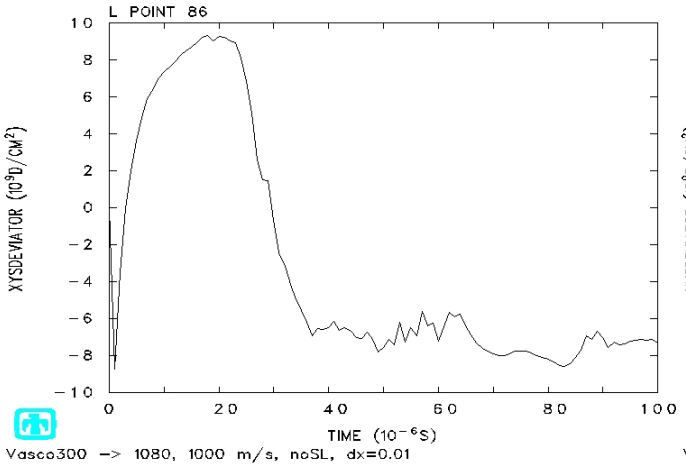

a) No Slide Line

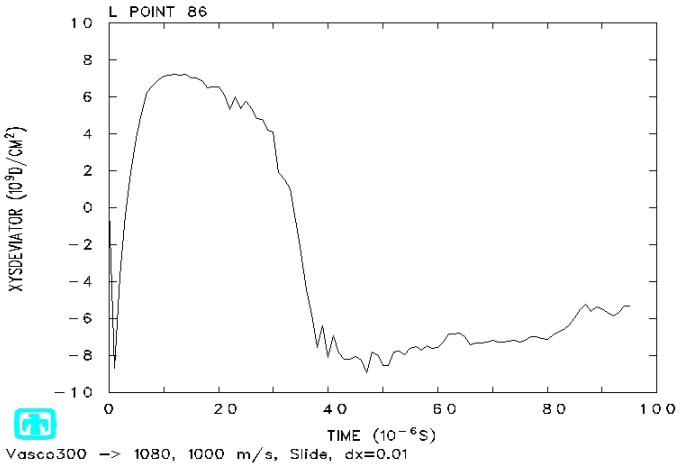

b) Slide Line

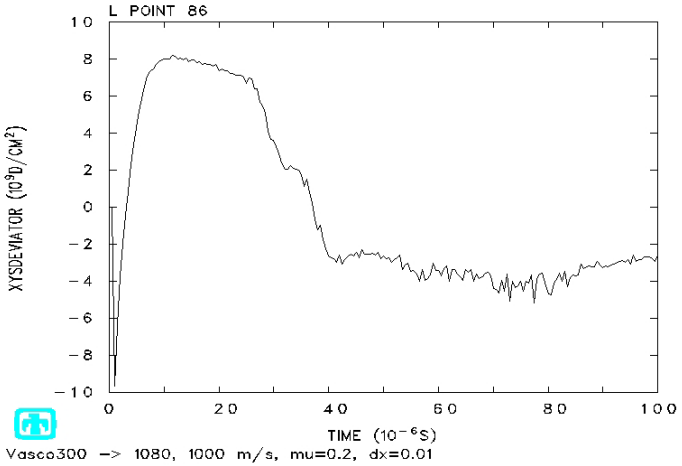

c) Boundary Layer

Figure 4.32 Tracer 86, Deviatoric Shear Stress History

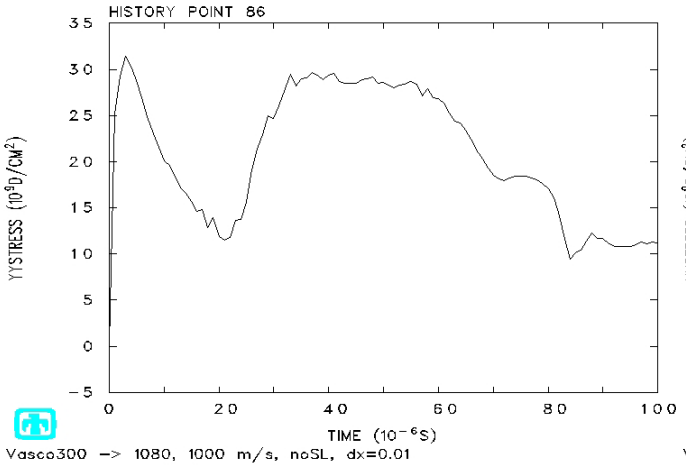

a) No Slide Line

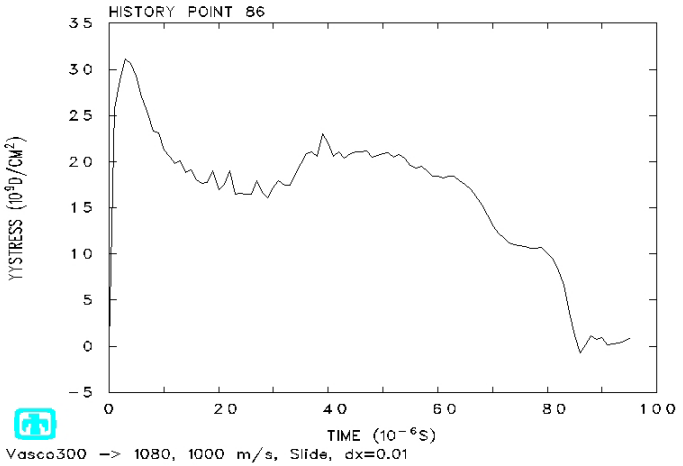

b) Slide Line

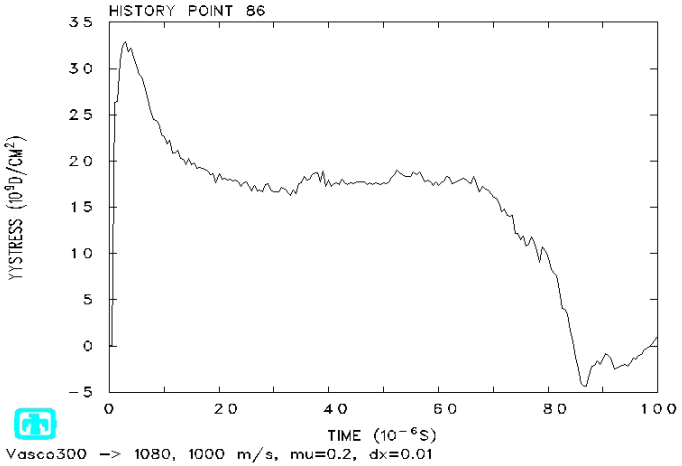

c) Boundary Layer

Figure 4.33 Tracer 86, Normal Stress History

The displacement plots of tracer 107 (Figure 4.34) show displacement magnitudes that are very similar for all three methods with final displacements differing by only .02cm or about 6% of the greatest displacement observed. The general displacement response is similar to that observed with tracer 86 except for an interruption observed in the 20 to 40 μs time interval for the No Slide Line method. Also, the small recovery after maximum displacement was reached that was observed previously is almost nonexistent for this tracer.

The temperature history for tracer 107 (Figure 4.35) also shows overall temperature responses similar to those observed for tracer 86 with the exception again of the No Slide Line method. A disruption in the temperature increase rate in the same 20 to 40 μs time interval for the No Slide Line method is observed. The temperature becomes very erratic in this time interval but still results in a steady final temperature of approximately 1225K. A much smaller disruption in the temperature development for the Slide Line method is also observed over the same time interval and the final temperature is approximately 975K, the smallest temperature increase. The temperature development for the Boundary Layer method appears relatively smooth and reaches a final temperature of approximately 1100K. While a temperature difference of only 125K was observed between the three methods for tracer 86, a higher difference of 250K, which is 27% of the largest temperature increase, is observed for tracer 107.

Figure 4.36 shows three very distinct pressure histories for tracer 107. Negative pressure values are indicated in the 20-40 μs time interval for the No Slide Line method while pressure values remain clearly positive for the other two methods. The maximum

pressure of 2.5GPa occurs with the Slide Line method but all three methods do show a trend towards a final pressure value of 1GPa.

The deviatoric shear stress history of tracer 107 (Figure 4.37) is roughly similar to that of tracer 86 (Figure 4.32) although no initial negative shear spike is observed. Additionally, compared to the shear stress magnitudes observed for tracer 86, the final shear stress magnitude is twice as large for the Boundary Layer method, but less than one half of the magnitude for the Slide Line method, and only one fourth of the magnitude for the No Slide Line method.

The y-component of normal stress for tracer 107 (Figure 4.38) shows a time response very similar to the pressure response. There is also more similarity between results for the Slide Line method and the Boundary Layer method. The largest peak value of 3.5GPa occurs with the Slide Line method but the No Slide Line method results in the largest final value of 1.8GPa. It should also be noted that these stress values are consistently greater in magnitude than the pressure values.

These tracer particle history plots would suggest that while the three different material interface methods do not produce significantly different overall effects in an impact scenario, there are significant differences that exist on a smaller, localized scale.

The reason for the curious results observed with the No Slide Line method in the 20 - 40 μs time interval is not readily apparent but looking back at Figure 4.26 reveals a projectile deformation state that may suggest a cause. Since the two materials are joined at the contact surface in the No Slide Line method, projectile material is pulled along with the target material and folds over on itself in the 20-40 μs time interval. This secondary impact would

definitely affect the displacement rate of material in the vicinity of tracer 107. Since the two other methods allow for relative material sliding, this effect is not observed.

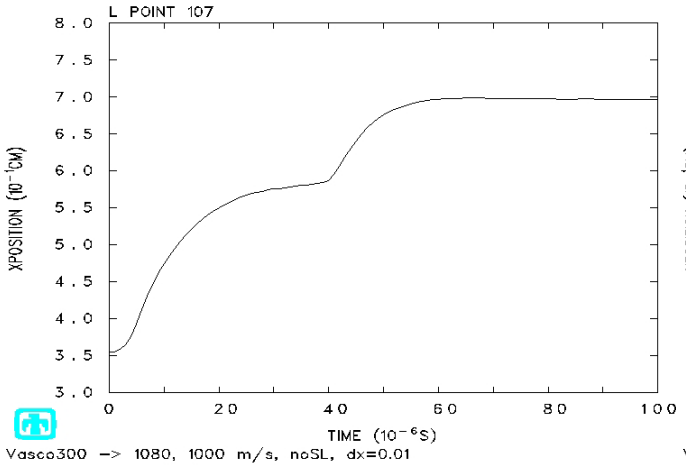

a) No Slide Line

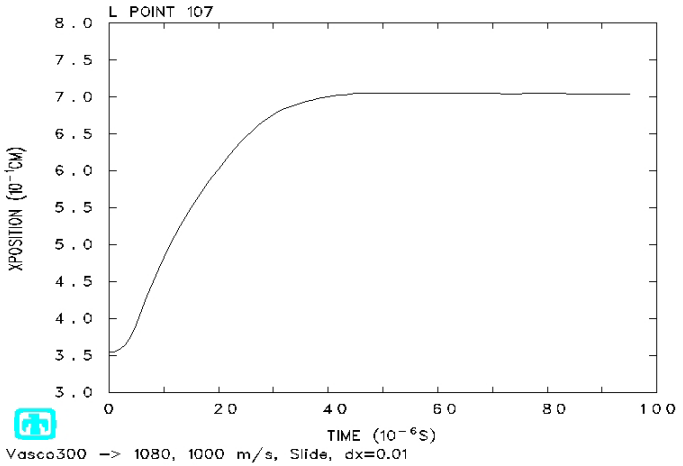

b) Slide Line

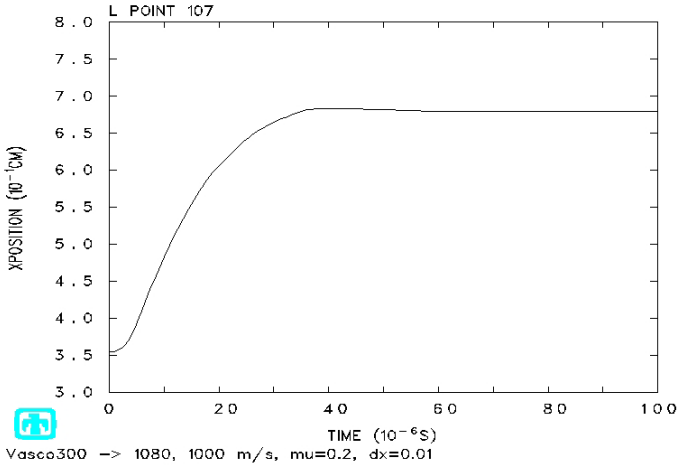

c) Boundary Layer

Figure 4.34 Tracer 107, x-Coordinate History

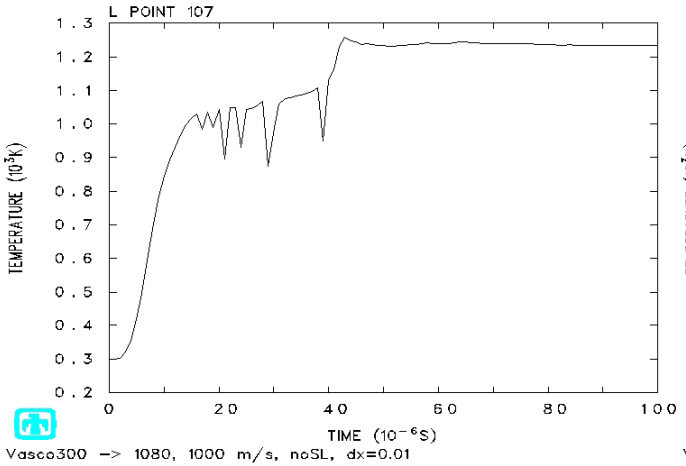

a) No Slide Line

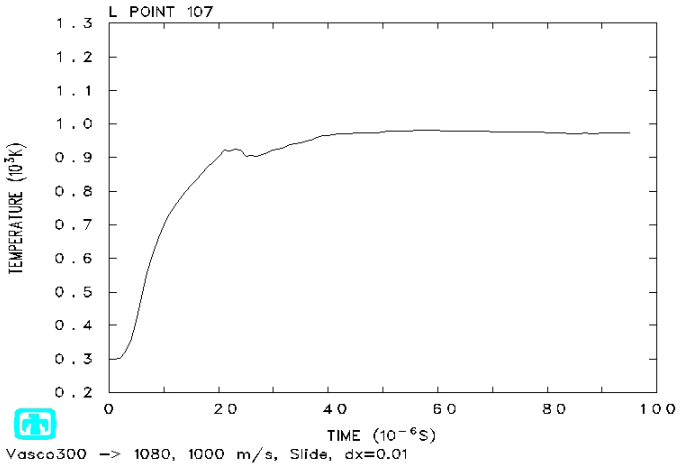

b) Slide Line

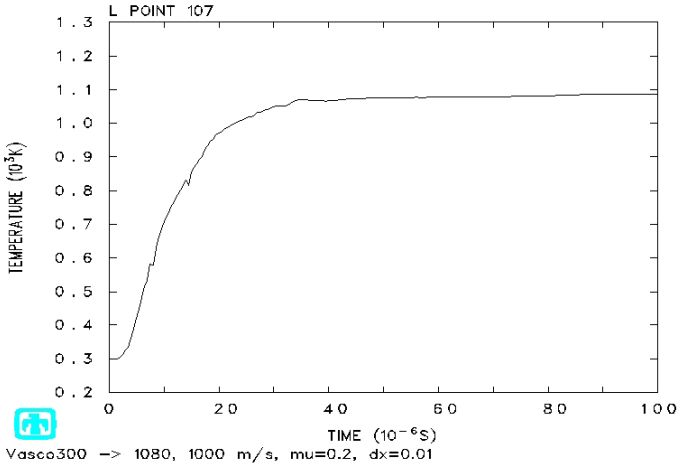

c) Boundary Layer

Figure 4.35 Tracer 107, Temperature History

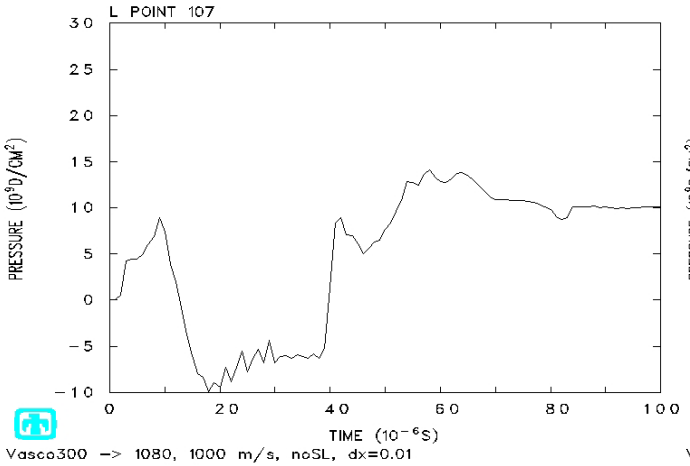

a) No Slide Line

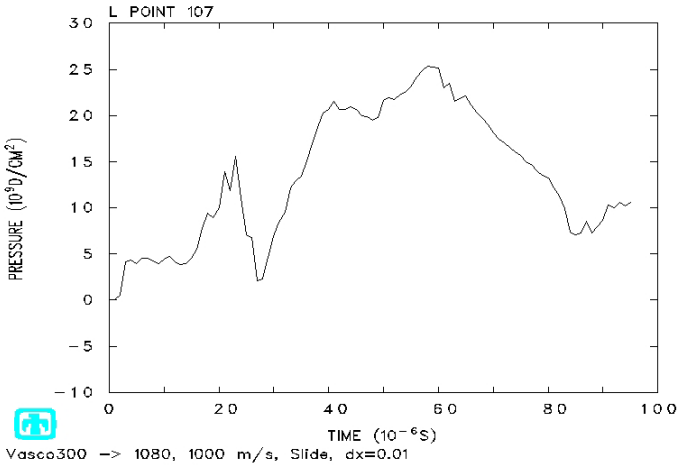

b) Slide Line

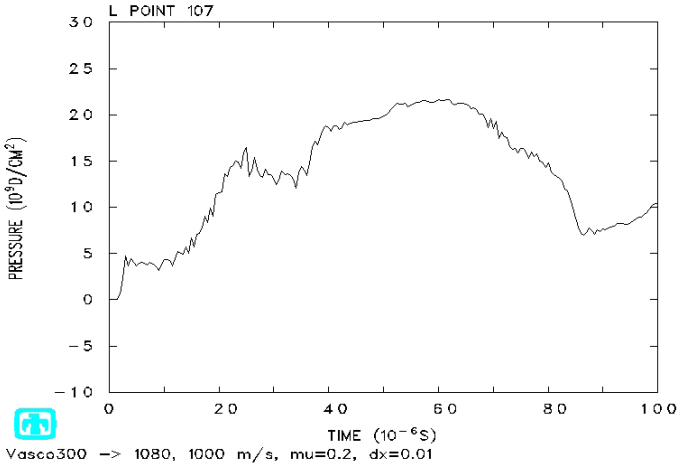

c) Boundary Layer

Figure 4.36 Tracer 107, Pressure History

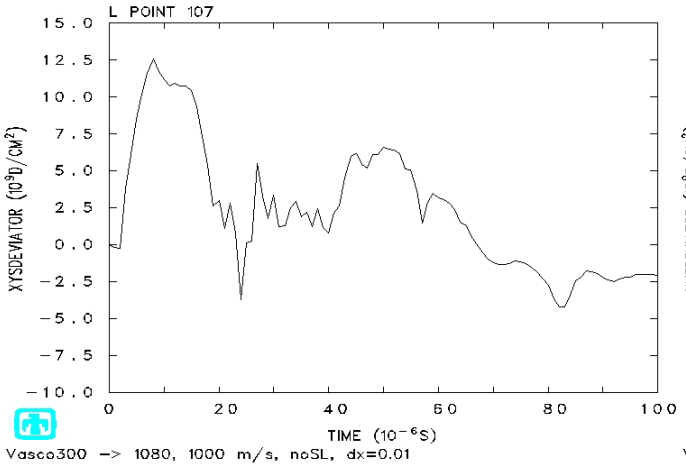

a) No Slide Line

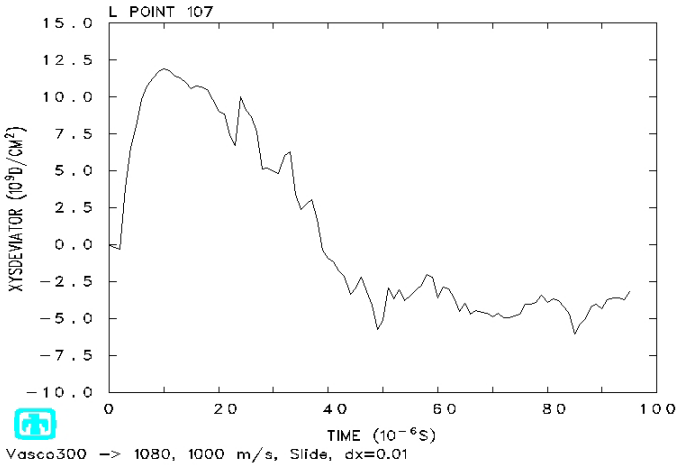

b) Slide Line

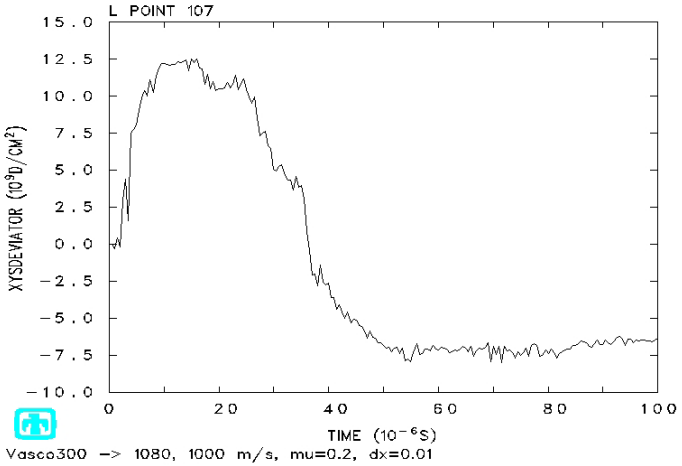

c) Boundary Layer

Figure 4.37 Tracer 107, Deviatoric Shear Stress History

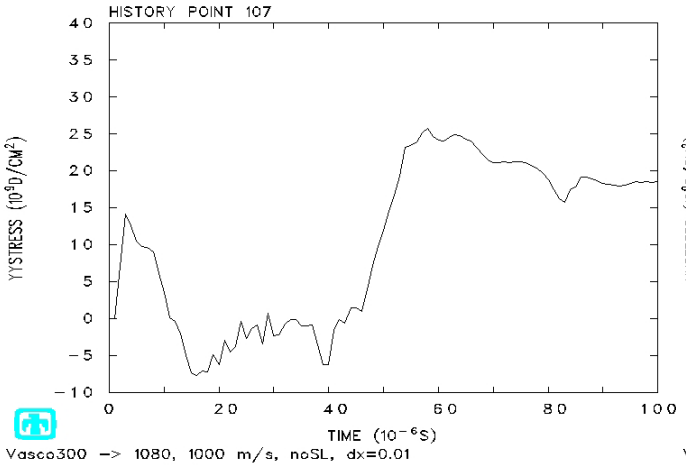

a) No Slide Line

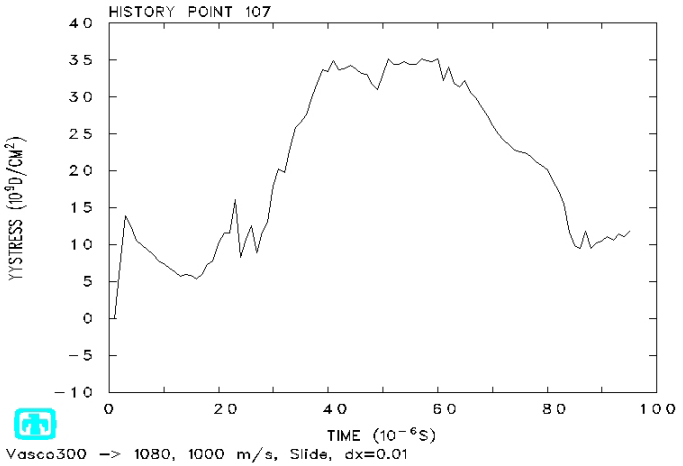

b) Slide Line

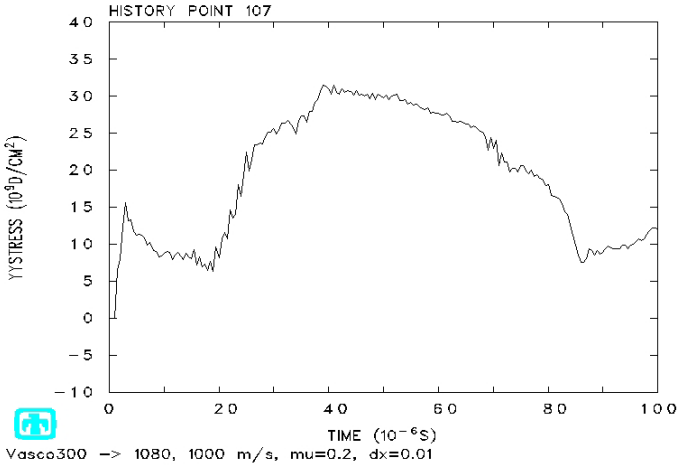

c) Boundary Layer

Figure 4.38 Tracer 107, Normal Stress History

Pure Sliding Results

The scenario of pure sliding reveals severe difficulties with the Slide Line method. Since this method establishes a frictionless sliding interface at the contact surface, we would not expect any shear stress to develop. However, a plot of the deviatoric shear stress reveals the development of a shear response throughout the projectile and target within the first few microseconds as can be seen in Figure 4.39. This development must be attributed to numerical noise. As the solution develops, this numerical noise dominates the solution and begins to generate completely nonphysical results. Thermodynamic warnings are prevalent again and the solution actually terminates at approximately 49 μs when the number of warnings exceeds one million. The dark blue cells seen in Figure 4.40 of the temperature profile indicates regions where the temperature has dropped below ambient. With no heat transfer considered, this must surely be a nonphysical result. Aside from the fact that the Slide Line method is inappropriate for this particular scenario, any other comments would be unwarranted.

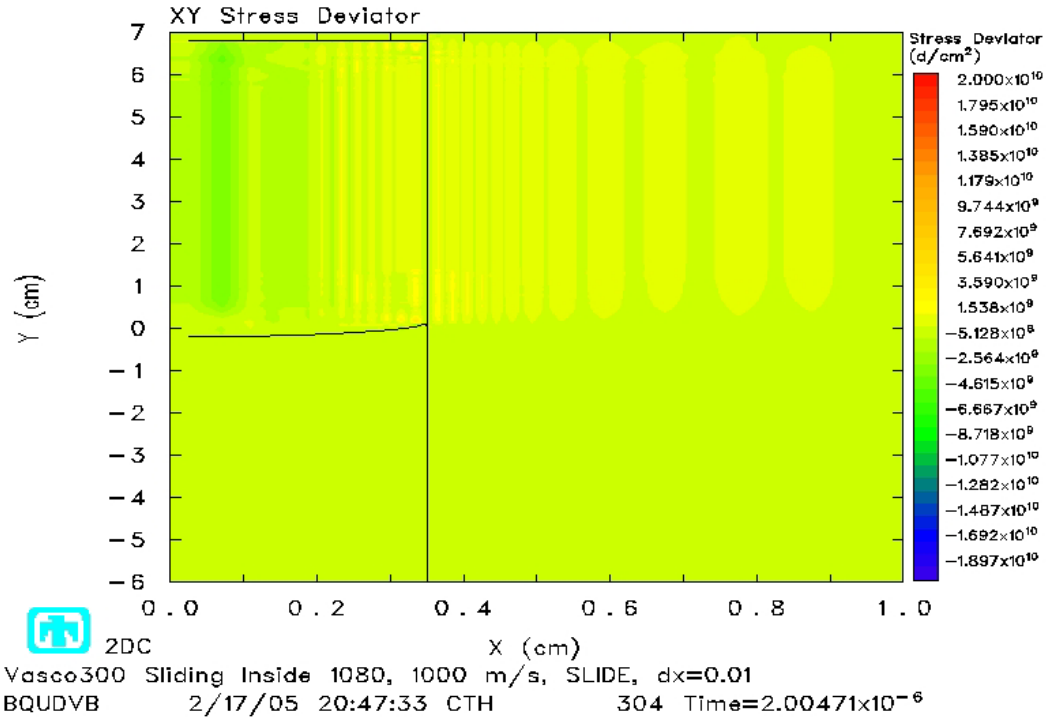

Figure 4.39 Deviatoric Shear Stress at 2 µs, Slide Line

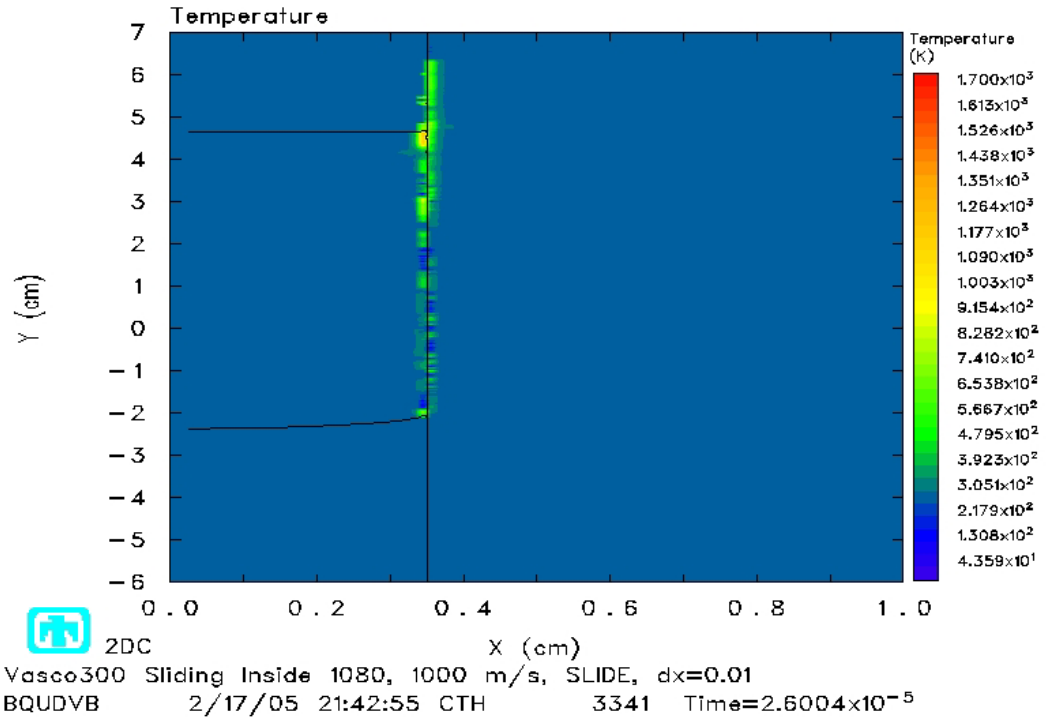

Figure 4.40 Temperature at 26 µs, Slide Line

Plots of the deviatoric shear stress for the other two methods reveal two very distinct developments. Figures 4.41a and 4.41b show shear stress states at 24 microseconds and 50 microseconds for the No Slide Line method. The shear response seen as alternating vertical regions of positive and negative shear is extensive in both the projectile and the target. As the solution progresses, this shear pattern in the target and the shear response itself weakens and begins to disappear, while the shear pattern in the projectile appears to intensify. In addition, the shear response in the projectile also shows alternating horizontal regions of positive and negative shear originating near the projectile nose. The shear development for the Boundary Layer method shown in figures 4.42a and 4.42b show a very intense region of shear in the target material near the material interface. This should be the effect of the friction body force which is added through the Boundary Layer Algorithm. The lack of other significant shear response features is attributed to the slip layer which would not transfer shear into the target and produce the material response seen with the No Slide Line method.

The shear response pattern could also be a result of numerical noise due to mesh size issues. The mesh cell size of .01cm for this case was carried over from the impact studies and may not be sufficient to capture the true material response for this scenario.

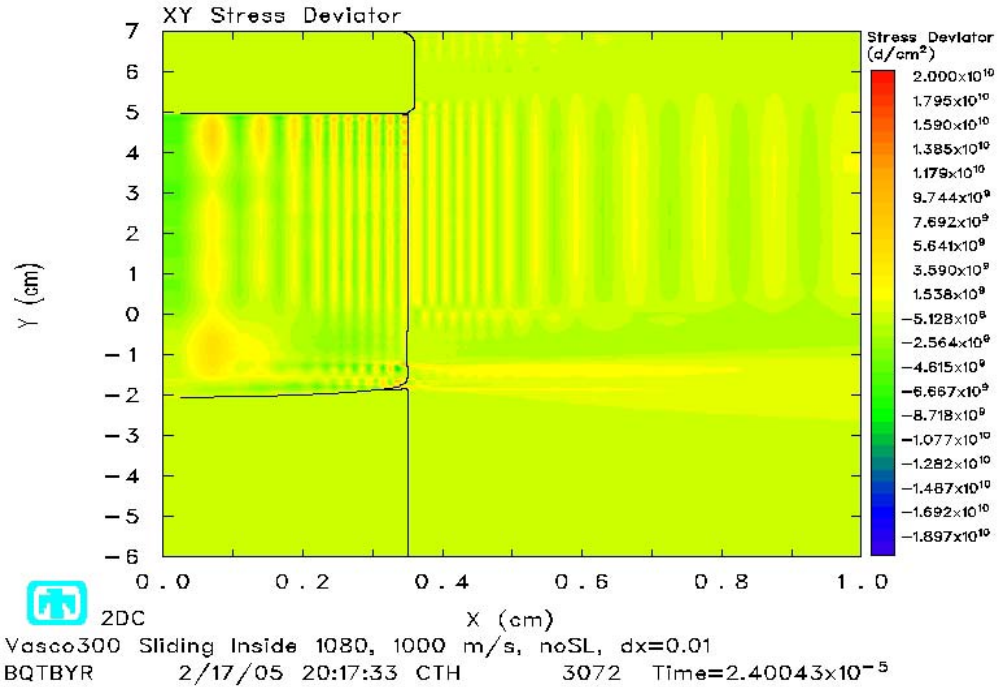

Figure 4.41a Deviatoric Shear Stress at 24 µs, No Slide Line

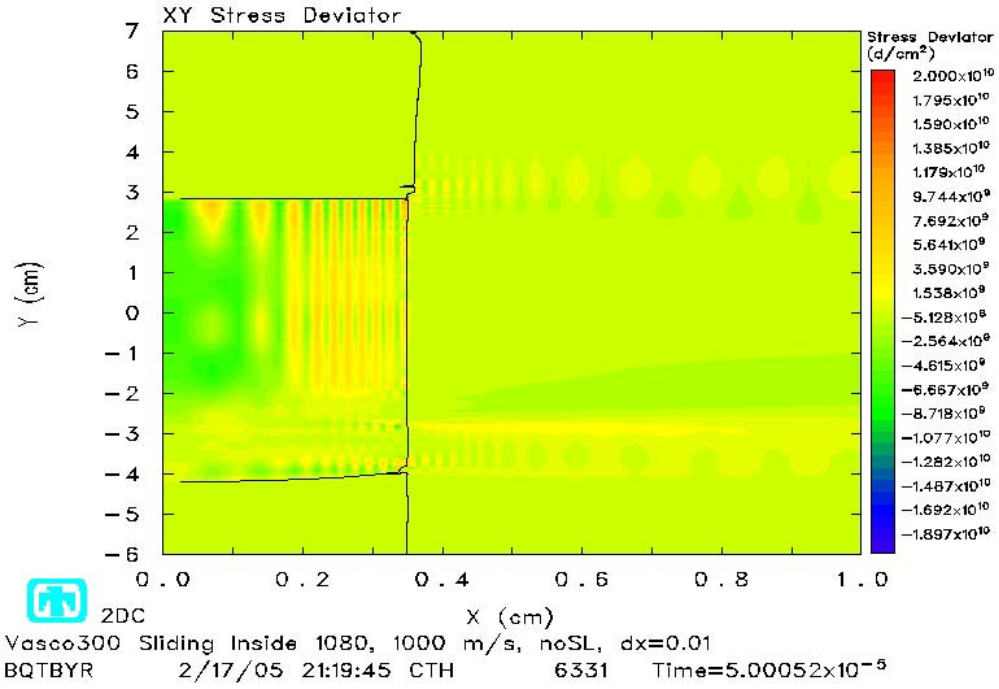

Figure 4.41b Deviatoric Shear Stress at 50 µs, No Slide Line

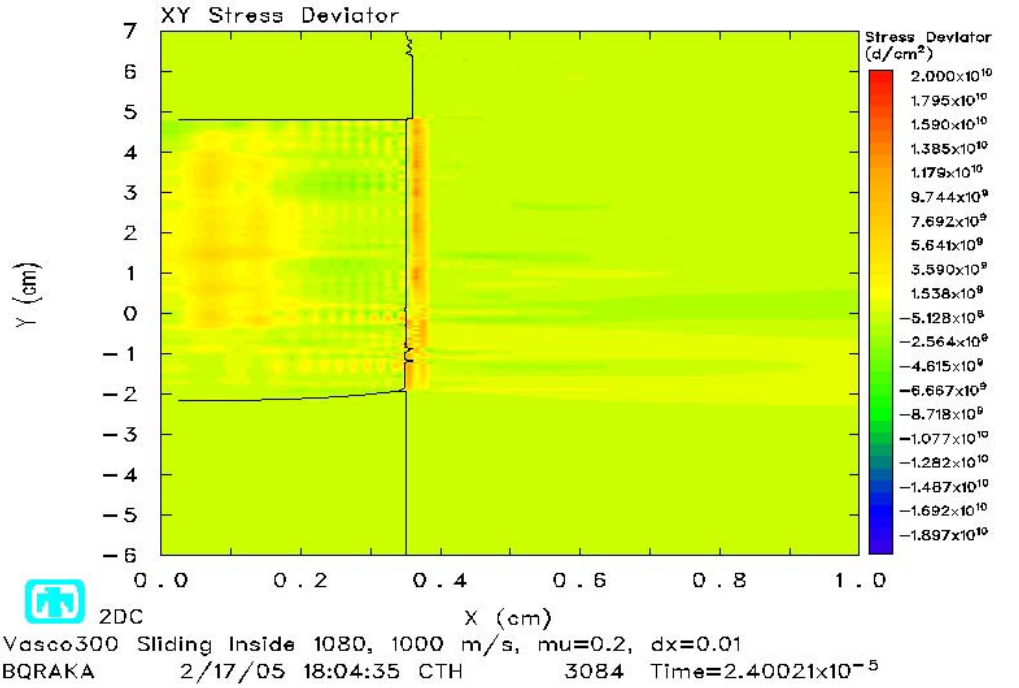

Figure 4.42a Deviatoric Shear Stress at 24 µs, BOUNDARY LAYER

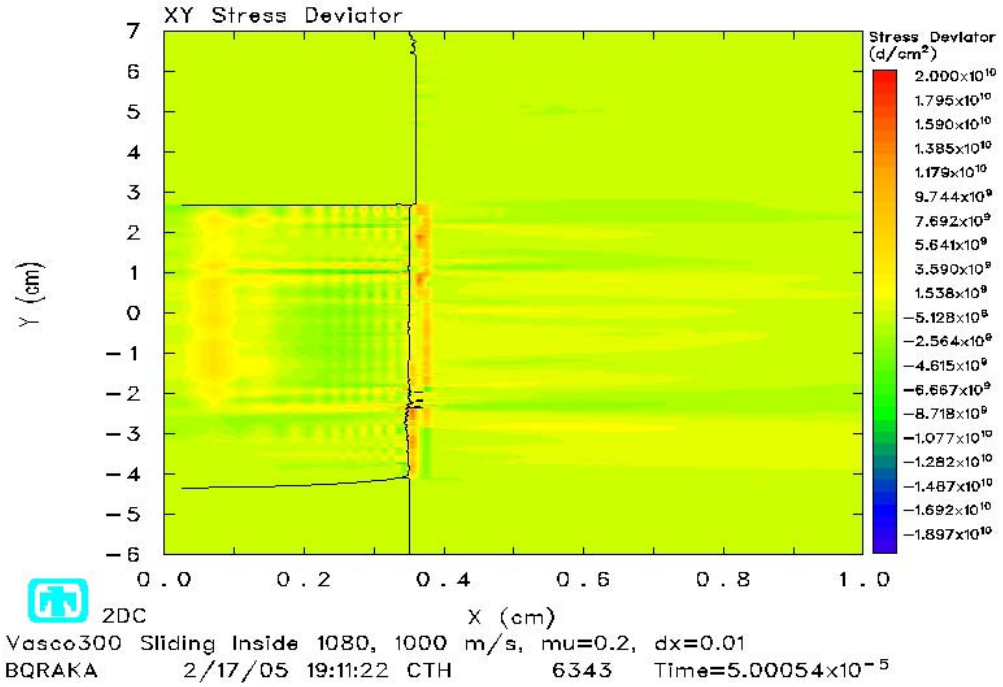

Figure 4.42b Deviatoric Shear Stress at 50 µs, BOUNDARY LAYER

The temperature development for the No Slide Line method and the Boundary Layer method are similar in magnitude and distribution as shown in Figures 4.43a and 4.43b. While the No Slide Line method produces a smoother temperature distribution, both methods produce a high temperature projectile surface layer near the leading edge which transitions into the target surface. It is somewhat surprising that the two fundamentally different methods would produce such similar results. The dissipation of shear stress in the target observed with the No Slide Line method along with the established layer of high temperature target material suggests the formation of a fluid layer. As this fluid layer grows, less shear stress is transferred into the target. It would appear that given enough time, both the No Slide Line method and Boundary Layer method will generate the same solution.

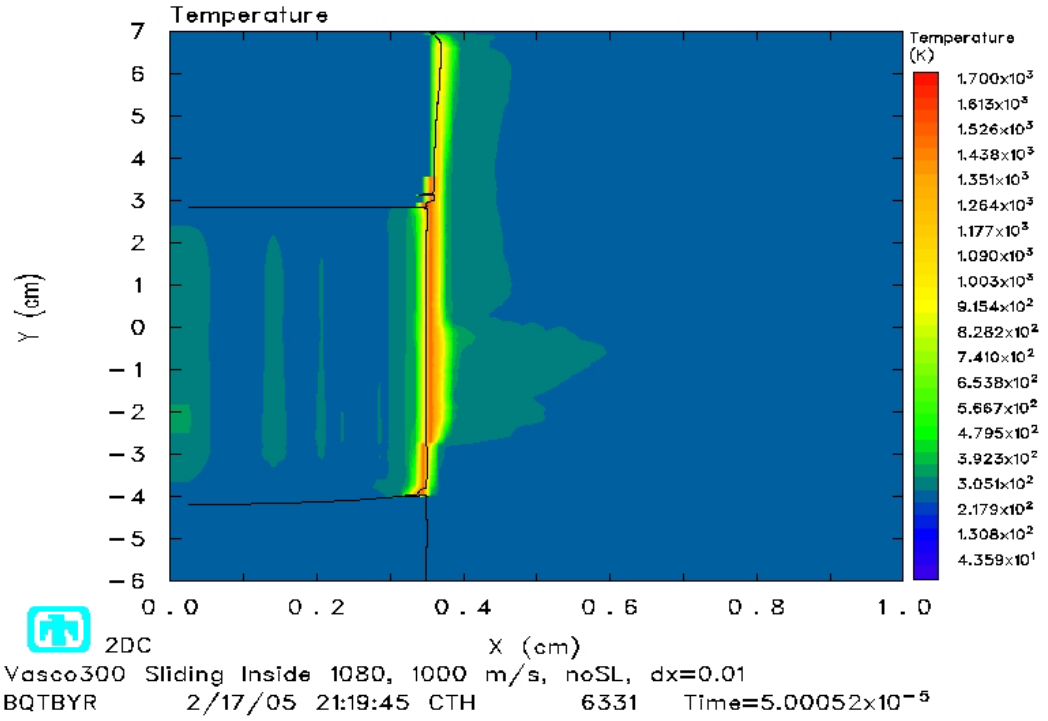

Figure 4.43a Temperature at 50 μs, No Slide Line

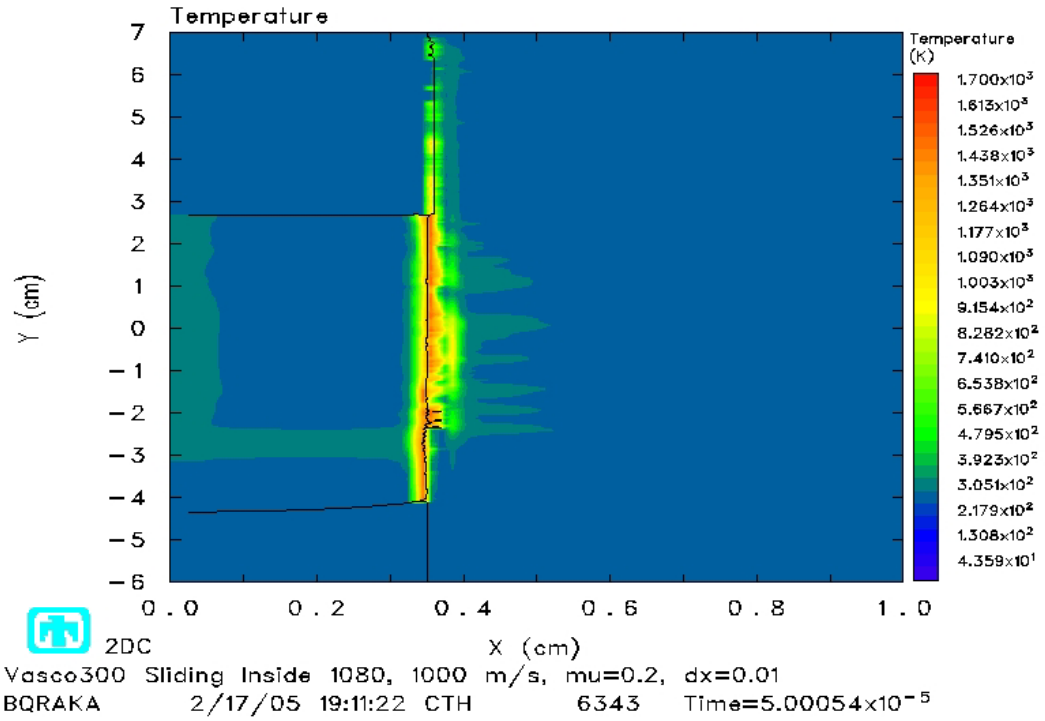

Figure 4.43b Temperature at 50 µs, Boundary Layer

V. Conclusions and Recommendations

Chapter Overview

Through the course of this thesis research, computational methods for the treatment of material interfaces available in the hydrocode CTH were investigated with the goal of establishing some criteria to aid in the application of these methods to scenarios for which they were not originally intended. The three methods investigated are repeated here:

1. No Slide Line, materials are joined at the contact surface
2. Slide Line, a frictionless sliding interface is implemented at the contact surface
3. Boundary Layer, friction is included and the sliding interface is shifted into the softer material

The specific application of interest is the simulation of the hypervelocity gouging phenomenon observed at the HHSTT.

Conclusions of Research

The first phase of this research analyzed a deep penetration impact event involving a steel projectile and an aluminum target. The projectile had a yield stress approximately six times that of the target and had nearly 3 times the stiffness. The resulting impact clearly showed an event dominated by target plastic deformation. For a relatively coarse mesh of .04cm, these impact studies indicated that the Boundary Layer method produced results that were the closest to experimental data. However, after refining the mesh to .01cm, the results were almost identical for all three methods. The effect of material interface phenomena in this scenario did not appear to be a significant

contributor to the impact solution. For this type of scenario then, the suggestion would be to use the No Slide Line method since it takes no effort on the part of the user to implement and requires the least computational effort.

The second phase of this research analyzed a normal impact event involving a Vascomax300 projectile and a 1080 steel target, in an attempt to model materials in use at the HHSTT. The projectile had a yield stress approximately three times that of the target but a stiffness value only 15% greater. The resulting impact showed significant plastic deformation of both the projectile and the target. Material interface effects were observed to produce detectable differences in the CTH solution. The No Slide Line method produced excessive deformation of the projectile in this scenario. Since the projectile was artificially joined to the target material at their contact surfaces, the higher plastic deformation rate of the target material pulled projectile material along with it. The Slide Line method produced results similar to the Boundary Layer method although the issue of thermodynamic warnings forced this solution to abort early which raises concerns about the accuracy of that solution. The Boundary Layer method produced results that were consistent with the other methods from an overall perspective but did not show any significant erratic phenomena in the tracer histories that were present in the other two methods. Even though it was observed that the Boundary Layer method was artificially increasing the yield strength of the projectile, the effect was relatively small. The Boundary Layer method appears to be the method of choice in this scenario since it is numerically stable and the user has some options with this method to fine tune the solution to reflect experimental data if available. Once a sufficiently similar simulation is

established, other aspects of the event of interest which were not physically observable can be studied in simulations with greater confidence.

The third phase of this research analyzed a sliding scenario involving a Vascomax300 projectile and 1080 steel target. This extreme scenario which attempts to isolate the ability of the three methods to model pure sliding produced some unexpected results. The numerical instability of the Slide Line method was made quite evident with this scenario. The similarities between the No Slide Line method and the Boundary Layer method were not at all expected. The issue of mesh refinement however precludes any definitive comparison of the two methods. Although the results do suggest that if the relative tangential velocity between two materials is sufficiently high, then both methods are suitable for use which would lead to the recommendation of the No Slide Line method simply for ease of implementation and reduction in computational effort.

Based on these limited findings, the No Slide Line method would be recommended for general use in high energy impact studies. Due to the numerical instability encountered with the Slide Line method, its application should be limited. The Boundary Layer method is too limited in its application for 2D models. The lack of support for parallel data processing is also a major drawback with this method. Implementing it in a 2D non-axisymmetric problem won't generate an error and cause the CTH run to abort but the solution will not include any friction input the user may be interested in. Unless the problem is 2D axisymmetric and results with a relatively coarse mesh are acceptable, so that solutions can be obtained with a standalone workstation, the Boundary Layer method offers no advantage.

This leads to a recommendation for simulations of the hypervelocity gouging problem at the HHSTT. For the 2D plane strain model currently in use, the No Slide Line method should be implemented. If there is interest in applying the Boundary Layer method for its capability to explicitly add a friction force to the problem then a 3D model will need to be created.

Recommendations for Future Research

This research has by no means been exhaustive in its attempt to discern which material interface methods are suitable for which situations. The recommendations for future research are:

1. Evaluate the three methods in oblique impact scenarios.
2. Evaluate the three methods in impact scenarios with coatings.
3. Evaluate the three methods for a 3D impact model.

Any future research effort should also implement the heat transfer capabilities of CTH in order to capture the extent to which friction affects the thermodynamic state of the materials.

Appendix: CTH Input File for Impact Scenario Two

```
*eor* cgenin
*
*This is the combined CTHGen/CTH input file
*This is the CTHGen input section
*
Vasco300 -> 1080, 1000 m/s, mu=0.2, dx=0.01
*
*All output from CTHGen will have this title
*This is the impact scenario of a Vascomax300 projectile impacting a
*1080 steel target at 1000 m/s, implementing the boundary layer method
*with a coefficient of friction of 0.2, and a .01cm mesh cell size in
*the area of interest
*
control
 mmp
 ep
 vpsave
endcontrol
*
mesh
 block geom=2dc type=e
*
* 2D-cylindrical coordinates, eulerian mesh
* axisymmetric problem, so only half model generated
*
  x0=0.
   x1 dxf=0.01 dxl=0.01 w=.5
   x2 dxf=0.01 dxl=0.04 w=5.5
  endx
*
*x ranges from 0. to 6.
*dxf is size of first cell in the range
*dxl is size of last cell in the range
*
  y0=-10.0
   y1 dyf=0.04 dyl=0.04 w=4.
   y2 dyf=0.04 dyl=0.01 w=2.
   y3 dyf=0.01 dyl=0.01 w=6.
   y4 dyf=0.01 dyl=0.04 w=2.
   y4 dyf=0.04 dyl=0.04 w=3.5
  endy
*
*y ranges from -10. to 7.5
*dyf is size of first cell in the range
*dyl is size of last cell in the range
*
 xactive 0 0.5
 yactive -1 7.5
*
*this is the initial mesh region containing activity
*helps speed up the computation by not working on the entire mesh from
*the start
```

```
*
 endb
endmesh
*
insertion of material
  package projectile
*
* main body of Vasacomax300 projectile, 7.11mm diameter, 71.1mm length
*
   material 2
   numsub 50
   xvel 0.0
   yvel -1000.e2
*
*  cgs units, cm/s
*
   insert box
    p1 0. 0.3555 p2 0.3555 7.1476
   endinsert
*
* only one insert allowed per package
*
  endpackage
  package projectile
*
* hemispherical nose of the Vasacomax300 projectile
*
   material 2
   numsub 100
   xvel 0.0
   yvel -1000.e2
   insert circle
    cen 0. 0.3555 rad 0.3555
   endinsert
  endpackage
  package target
*
* 1080 Steel target, 152mm diameter, 198mm length
*
   material 1
   numsub 100
   xvel 0.
   yvel 0.
   insert box
    p1 0. -19.8
    p2 7.6 0
   endinsert
  endpackage
endinsertion
*
edit
 expanded
endedit
*
```

```
eos
 mat1 ses iron
 mat2 ses Steel_V300
*
* Sesame Equation of State tables, limited material selection
*
endeos
*
epdata
 vpsave
 mix 3
*
*calculate yield strength in mixed cells using volume
*averaged yield strength normalized by the sum of the
*volume fractions of the materials that can support shear
*
 matep 1
  johnson-cook IRON
  poisson 0.28
  yield=7.0e9
*
*Viscoplastic rate dependent model of Iron, closest material available
*to 1080 steel
*
 matep 2
  st=19
  poisson=0.27
  yield=14.47e9
*
*Viscoplastic rate independent model of Vascomax
*only some Steinberg-Guinan-Lund models are rate dependent
*
 BLINT 1 soft 1 hard 2 csl 1.5 cbl 1.5 fric 0.2 corr
*
*Boundary Layer Interface model
*first number is an identifier for each BLINT entry, if you have 3
*materials, you will need two BLINT entries uniquely identified
*soft 1, material identifier of the soft material
*hard 2, material identifier of the hard material
*csl 1.5, slip layer width is 1.5 cell diagonals
*cbl 1.5, boundary layer width is 1.5 cell diagonals
*fric 0.2, coefficient of friction is 0.2
*corr, increases hard material yield stress by a factor proportional to
*      the increased radius of the projectile due to soft material gain
*      in mixed material cells
*
ende
*
tracer
*
*tracer input, starting x,y coord. to ending x,y coord.
*n = total number of tracers to distribute including the end pts.
*
*Centerline
```

```
 add 0. 0. to 0. 7.0 n 8
 add 0. 7.25
*projectile nose boundary layer
 add .005 .005 to .405 .005 n=9
 add .005 .015 to .405 .015 n=9
 add .005 .025 to .405 .025 n=9
 add .005 .035 to .405 .035 n=9
 add .005 .045 to .405 .045 n=9
 add .005 .055 to .405 .045 n=9
 add .005 .105 to .405 .105 n=9
 add .005 .205 to .405 .205 n=9
 add .005 .305 to .405 .305 n=9
 add .005 .405 to .405 .405 n=9
 add .005 .505 to .405 .505 n=9
*target boundary layer
 add .005 -.005 to .405 -.005 n=9
 add .005 -.015 to .405 -.015 n=9
 add .005 -.025 to .405 -.025 n=9
 add .005 -.035 to .405 -.035 n=9
 add .005 -.045 to .405 -.045 n=9
 add .005 -.055 to .405 -.055 n=9
 add .005 -.105 to .405 -.105 n=9
 add .005 -.205 to .405 -.205 n=9
 add .005 -.305 to .405 -.305 n=9
 add .005 -.405 to .405 -.405 n=9
 add .005 -.505 to .405 -.505 n=9
endt
matplot
 x=0.,.5
 y=-1.,1.
Endm
*
*generates a plot of materials in the metamat file
*use popx11 command to view file or popjpg command to make a jpeg
*
matplot
 x=0.,5.
 y=-3.,7
endm
************************************************************
*eor* cthin
*
*CTH input section
*
Vasco300 -> 1080, 1000 m/s, mu=0.2, dx=0.01
*
*All output from CTH will have this title
*
control
 mmp
 tstop = 200.0e-6
 nscycle = 150000
 cpshift=600.
 ntbad=1000000
```

```
*
*mmp allows multiple pressures and temperatures in mixed material cells
*tstop = solution end time
*nscycle = solution will end if number of cycles is exceeded
*cpshift = allows extra time for CTH to write data
*ntbad = maximum thermodynamic warnings before CTH aborts
*
endc
*
convct
 interface=high_resolution
endc
*
edit
 shortt
  time=0. dt=20.e-6
*
*restart data will be written every “dt” seconds
*
 ends
 longt
  tim=0 dt=1.0
*
*restart data will be written every “dt” seconds
*
 endl
 histt
  time=0 dt=0.5e-6
  htracer all
*
*history data will be written to hcth every “dt” seconds
*data for all tracer points is written
*
 endh
 plott
  time=0 dt=1.e-6
  time=50.e-6 dt=2.e-6
  time=100.e-6 dt=5.e-6
*
*cthplot data is written to restart file every “dt” seconds
*starting at “time”
*beware restart file size limit is 2GB
 endp
ende
*
boundary
 bhydro
   bxb=0. bxt=1. byb=1. byt=1.
*
*symmetry boundary condition at minimum x
*sound speed absorbing boundary condition at max x, min y, and max y
*equivalent to semi-infinite boundary
*
 endh
```

```
endb
*
mindt
 time 50.0e-6
 dtmin 1.0e-9
endm
*
*CTH will abort if the time step drops below dtmin after “time”
*
```

References

1. Anderson, C. E. "An Overview of the Theory of Hydrocodes," *International Journal of Impact Engineering*, Vol. 5: 33-59 (1987).

2. Barber, John P., and Bauer, David P. "Contact Phenomena at Hypervelocities," *Wear*, 78: 163–169, 1982.

3. Bayer, Raymond G. *Mechanical Wear Fundamentals and Testing*, New York: Marcel Dekker, Inc., 2004.

4. Bell, R.L. et al. *CTH User's Manual and Input Instructions, Version 6.01*. Sandia National Laboratories, Albuquerque NM, 2003.

5. Bell, R.L. et al. *CTHGEN User's Manual and Input Instructions, Version 5.00*. Sandia National Laboratories, Albuquerque NM, 2003.

6. Bowden, F.P. and E.H. Freitag. "The Friction of Solids at Very High Speeds," *Proceedings of the Royal Society* 248: 350–367 (1958).

7. Forrestal, M. J., Bar, N. S., and Luk, V.K. "Penetration of Strain-Hardening Targets With Rigid Spherical-Nose Rods," *Journal of Applied Mechanics*, Vol. 58: 7-10 (1991).

8. Forrestal, M. J., Okajima, K., and Luk, V.K. "Penetration of 6061-T651 Aluminum Targets With Rigid Long Rods," *Journal of Applied Mechanics*, Vol. 55: 755-760 (1988).

9. Laird, David J. *The Investigation of Hypervelocity Gouging* AFIT/DS/ENY 02-01, PhD dissertation, Air Force Institute of Technology, Wright-Patterson AFB OH, March 2002.

10. Laird, David J., and Palazotto, Anthony N. "Gouge Development During Hypervelocity Sliding Impact," *International Journal of Impact Engineering*, Vol. 30: 205-223 (2004).

11. McGlaun, J. M., and Thompson, S. L. "CTH: A Three-Dimensional Shock Wave Physics Code," *International Journal of Impact Engineering*, Vol. 10: 351-360, (1990).

12. Saada, Adel S. *Elasticity: Theory and Applications, 2nd Edition*. Malabar FL: Krieger Publishing Company, 1993.

13. Silling, Stewart A. *CTH Reference Manual: Boundary Layer Algorithm for Sliding Interfaces in Two Dimensions*. Sandia National Laboratories, Albuquerque NM, 1994.

14. Szmerekovsky, Andrew G. *The Physical Understanding Of The Use Of Coatings To Mitigate Hypervelocity Gouging Considering Real Test Sled Dimensions* AFIT/DS/ENY 04-06, PhD dissertation, Air Force Institute of Technology, Wright-Patterson AFB OH, September 2004.

Vita

Captain Minh C. Nguyen graduated from Columbus Alternative High School in Columbus, Ohio in 1995. His undergraduate studies were conducted at the University of Southern California from 1995-1999 where he received a Bachelor of Science degree in Aerospace Engineering. He was commissioned thru AFROTC Detachment 060 at the University of Southern California in May 1999.

Prior to attending the Air Force Institute of Technology, he served with the A-10 System Program Office at Hill AFB, UT as a Mechanical Systems Engineer. During this time he was also trained as an Aircraft Battle Damage Engineer in support of the A-10. In September 2003, he entered the Graduate School of Engineering and Management, Air Force Institute of Technology. Upon graduation, he will be assigned to the Air Force Non Destructive Inspection Lab at Tinker AFB, Oklahoma.

REPORT DOCUMENTATION PAGE

Form Approved
OMB No. 074-0188

1. REPORT DATE *(DD-MM-YYYY)*	**2. REPORT TYPE**	**3. DATES COVERED** *(From – To)*
21-03-2005	Master's Thesis	Aug 2003 – March 2005

4. TITLE AND SUBTITLE

Analysis of Computational Methods for the Treatment of Material Interfaces

5a. CONTRACT NUMBER

5b. GRANT NUMBER

5c. PROGRAM ELEMENT NUMBER

6. AUTHOR(S)

Nguyen, Minh C., Captain, USAF

5d. PROJECT NUMBER

5e. TASK NUMBER

5f. WORK UNIT NUMBER

7. PERFORMING ORGANIZATION NAMES(S) AND ADDRESS(S)

Air Force Institute of Technology
Graduate School of Engineering and Management (AFIT/EN)
2950 Hobson Way, Building 640
WPAFB OH 45433-8865

8. PERFORMING ORGANIZATION REPORT NUMBER

AFIT/GAE/ENY/05-M15

9. SPONSORING/MONITORING AGENCY NAME(S) AND ADDRESS(ES)

Air Force Office of Scientific Research (AFRL/AFOSR)
Attn: Dr Neal D. Glassman
4015 Wilson Boulevard, Room 713
Arlington, VA 22203-1954

10. SPONSOR/MONITOR'S ACRONYM(S)

11. SPONSOR/MONITOR'S REPORT NUMBER(S)

12. DISTRIBUTION/AVAILABILITY STATEMENT

APPROVED FOR PUBLIC RELEASE; DISTRIBUTION UNLIMITED.

13. SUPPLEMENTARY NOTES

14. ABSTRACT

Rocket sled tests at the Air Force Research Laboratory's Holloman High Speed Test Track frequently approach velocities where gouging development becomes the limiting factor to achieving higher operating velocities. Direct observation of the gouging process is not possible so computational modeling is necessary to study the phenomenon. Since gouging development is dependent on the impact surface conditions, the method used to model material interfaces directly affects the accuracy of the solution. Three methods are available in the hydrocode CTH to handle material interfaces: 1) materials are joined at the interface, 2) a frictionless slide line is inserted, and 3) a boundary layer interface is established. An axisymmetric impact scenario is used to explore these methods and their influence on high energy impact solutions. The three methods are also compared in an axisymmetric sliding scenario. The method of joining materials at the contact surface appears well suited to the simulation of high energy impact events. The frictionless slide line method produces significant numerical instability, while the boundary layer interface method is too limited for two dimensional applications.

15. SUBJECT TERMS

hypervelocity gouging, high energy impact, friction, material interfaces, hydrocodes

16. SECURITY CLASSIFICATION OF:			**17. LIMITATION OF ABSTRACT**	**18. NUMBER OF PAGES**	**19a. NAME OF RESPONSIBLE PERSON**
a. REPORT	**b. ABSTRACT**	**c. THIS PAGE**			Dr Anthony N. Palazotto
U	**U**	**U**	**UU**	105	**19b. TELEPHONE NUMBER** *(Include area code)* (937) 785-3636, ext 4599

Standard Form 298 (Rev. 8-98)
Prescribed by ANSI Std. Z39-18